Generalized Image and Video Quality Assessment using Prompt-Guided Latent Diffusion Models

Anonymous authors
Paper under double-blind review

Abstract

The design of image and video quality assessment (QA) algorithms is extremely important to benchmark and calibrate user experience in modern visual systems. A major drawback of the state-of-the-art QA methods is their limited ability to generalize across diverse image and video data with reasonable distribution shifts. In this work, we leverage the denoising process of diffusion models for generalized image QA (IQA) and video QA (VQA) by understanding the degree of alignment between learnable quality-aware text prompts and images or video frames. In particular, we learn cross-attention maps from intermediate layers of the denoiser of latent diffusion models (LDMs) to capture quality-aware representations of images or video frames. Since applying text-to-image LDMs for every video frame is computationally expensive for videos, we only estimate the quality of a frame-rate sub-sampled version of the original video. To compensate for the loss in motion information due to frame-rate sub-sampling, we propose a novel temporal quality modulator. Our extensive cross-database experiments across various user-generated, synthetic, low-light, frame-rate variation, ultra high definition, and streaming content-based databases show that our model can achieve superior generalization in both IQA and VQA.

1 Introduction

The proliferation of mobile devices with image and video capturing capabilities has led to an explosion in the number of images and videos captured, stored and shared on various platforms. This has necessitated quality assessment (QA) of images and videos. QA algorithms are broadly classified into three major categories, namely full-reference QA, reduced-reference QA and no-reference QA. 1) Full-reference QA: Here, the pristine/undistorted version of the inference image/video is also available. Examples of such measures include SSIM Wang et al. (2004), and VMAF Rassool (2017). 2) Reduced-reference QA: Here, only some partial information about the pristine version of the inference image/video is also available. RRED Soundararajan & Bovik (2011) and ST-RRED Soundararajan & Bovik (2013) are examples of such methods. 3) No-reference QA: Here, only the inference image/video is available for quality assessment. NR QA has applications in assessing the quality of images/ videos that are captured using various camera devices, where a pristine version of that image/ video is absent.

Several classical NR algorithms for image QA (IQA) (Mittal et al., 2012) and video QA (VQA) (Saad et al., 2014), suffer in their ability to model a wide range of distortions. The emergence of deep neural networks (DNN) gave rise to a variety of NR-IQA (Ke et al., 2021; Su et al., 2020) and NR-VQA (Li et al., 2019a; 2021) methods. The DNN based methods suffer from a lack of generalization capability. Such models trained on a large dataset fail to predict image or video quality on other datasets accurately. For example, models trained on a large dataset with camera captured videos fail to generalize to varying evaluation scenarios such as diverse camera captures, varying frame rates, gaming videos, ultra high-definition and so on. Multi-modal vision-language models were recently shown to be promising for their generalizability for NR-IQA and NR-VQA. In particular, CLIP-IQA (Wang et al., 2023a) and BUONA-VISTA (Wu et al., 2023a) show the capacity of vision-language models to predict image and video quality respectively even in a zero-shot setting. Such models can achieve promising generalizability on par with IQA and VQA specific models

through a cost-effective prompt tuning method. These observations motivate the study of how to leverage existing large pretrained models to achieve generalizable NR-QA.

Recently, several pieces of work find that text-to-image (T2I) diffusion models show superior out of distribution generalization performance compared to vision language models on a variety of image retrieval, recognition, and reasoning tasks (He et al., 2023; Li et al., 2023a; Kawar et al., 2023; Ma et al., 2023). This makes them an interesting choice for achieving generalizable NR-QA. The reason for such generalization has been attributed to the inductive bias in the denoising architecture (Kadkhodaie et al., 2024). However, diffusion models are typically designed for generation of different image content conditioned on textual descriptions and their application to the QA task is non-trivial. In particular, arbitrary noise levels cannot help extract quality aware features. Moreover, since diffusion models are trained to exploit the textual prompts for generation, there is a need to understand how textual prompts can be used to extract quality-aware information.

In this work, we present Generalized IQA (**GenzIQA**) and Generalized VQA (**GenzVQA**) to explore the potential of prompt-guided T2I latent diffusion models (LDMs) for achieving generalizability in both NR-IQA and NR-VQA respectively. In particular, we leverage the generalization capability of diffusion models for the IQA task by using cross-attention finetuning, quality-aware prompt learning, and the design of suitable noise levels to extract quality-aware features from intermediate layers of the denoiser of the reverse diffusion process. We conduct a detailed analysis to show that there is a delicate choice of the noise to be added to the image when passed through the diffusion model to extract quality-aware features. Thus, our key contribution is to effectively leverage the generalization capabilities of LDMs for the IQA task. We show that our approach can achieve far superior generalization than any existing NR-IQA model on a variety of datasets. Applying such a T2I model to every video frame for VQA is computationally expensive. In this regard, we estimate the quality of the video at a lower frame-rate but compensate for the loss in motion information in the sub-sampled video. In particular, we propose a temporal quality modulator (TQM) that adjusts the predicted video quality by accounting for the loss of motion information. TQM estimates how the similarities of the visual features given by diffusion model with motion features of sub-sampled video differ from that of its similarities with the motion-features of original video. Our main contributions are summarized below:

- We design a unified framework for NR-IQA and NR-VQA to achieve the best generalizable performance among all existing methods across a variety of IQA and VQA datasets.
- We show that quality-aware tuning of cross-attention maps, extracted from the intermediate layers of the denoiser in the reverse diffusion process, in conjunction with quality-aware learning of contextual text prompts are necessary to render diffusion models effective for IQA and VQA.
- We propose a novel temporal quality modulator by computing the cross-attention between the sub-sampled video features of the LDM and the video motion features at original and sub-sampled frame rates. This allows the LDM to estimate video quality at reasonable compute times.
- We conduct a detailed analysis of the role of noise added to the latent variable during denoising and find that there exists a delicate relationship between the noise level and the ability of the denoiser for effective QA.
- We perform extensive experiments across 11 VQA and 6 IQA databases covering user-generated, restoration, variable frame-rate, Ultra-HD, and streaming video scenarios to establish the superior generalizability of our model with respect to existing models.

2 Related Work

2.1 Image Quality Assessment

Hand-crafted feature-based methods such as BRISQUE (Mittal et al., 2012), DIIVINE (Moorthy & Bovik, 2011) and BLIINDS (Saad et al., 2012), exploit the natural scene statistics while CORNIA (Ye et al., 2012)

and HOSA (Xu et al., 2016) design codebook learning-based methods. With the emergence of DNN, various end-to-end learning methods (Zhang et al., 2018c; Kim & Lee, 2016), or methods regressing pretrained convolutional neural network features (Zhang et al., 2018b; Zeng et al., 2017) against quality have been designed. Transformer-based models such as MUSIQ (Ke et al., 2021) and TReS (Golestaneh et al., 2022) also show promising performance on both synthetic and in-the-wild IQA tasks. MetaIQA (Zhu et al., 2020) proposes meta-learning for complex real-world distortions while HyperIQA (Su et al., 2020) proposes a hyper network to capture various distortion and semantic attributes in images. Recently, a few works employ diffusion models (Fu et al., 2024; Li et al., 2024b), but they involve training the entire diffusion model, thus increasing the computational complexity.

One approach to deal with generalization in IQA is by designing self-supervised quality representations through models such as CONTRIQUE (Madhusudana et al., 2022b), Re-IQA (Saha et al., 2023), and QPT (Zhao et al., 2023). CLIP-IQA (Wang et al., 2023a) is a vision-language model that shows very good zero-shot generalization for the IQA task. DEIQT (Qin et al., 2023) designs an attention-panel decoder learning with limited data samples. LIQE (Zhang et al., 2023a) trains a CLIP-based vision language model on six different databases, showing good performance in cross-database settings. TTA-IQA (Roy et al., 2023) uses the test-time adaptation technique to generalize a pretrained IQA model for different kinds of databases. Recently, GRepQ (Srinath et al., 2024) presents a self-supervised learning method that can lead to generalized quality representations. QCN (Shin et al., 2024) proposes a geometric order learning to achieve good cross-database performance in IQA. LoDa (Xu et al., 2024) adapts vision-transformers for IQA using another pre-trained CNN, while DSMix (Shi et al., 2024) proposes distortion-induced pre-training to enhance performance for existing IQA models. Recently, DiffV2IQA (Wang et al., 2025) proposed a dual branch model consisting of vision-transformer and ResNet50 to illustrate the correlation between diffusion model's ability to reconstruct an image and its quality. Also, PFD-IQA (Li et al., 2025) proposes IQA method by leveraging the denoising ability of a diffusion model to remove noise from quality-aware features. Despite these efforts, there is a need to consistently achieve better generalization across diverse and complex distortion types.

2.2 Video Quality Assessment

Classical approaches such as VBLIINDS (Saad et al., 2014) and VCORNIA (Xu et al., 2014) learn natural scene statistics of videos by modelling the discrete cosine transform. TLVQM (Korhonen, 2019) shows robust VQA performance by modelling temporal low complexity features with spatial high complexity features. VIDEVAL (Tu et al., 2021a) is an ensemble of various handcrafted features designed to capture diverse quality attributes in a video. Among DNN approaches, while VSFA (Li et al., 2019a) and MDTVSFA (Li et al., 2021) learn a gated recurrent unit on top of pretrained ResNet50 features (He et al., 2016), PVQ (Ying et al., 2021) learns an ensemble of ResNet50 trained on IQA and a 3D ResNet18 trained on action recognition tasks. CSVT-BVQA (Li et al., 2022) also transfers spatial knowledge from a pretrained IQA model and temporal knowledge from a pretrained action recognition model. Among transformer based models, FAST-VQA (Wu et al., 2022) learns an end-to-end model by spatially fragmenting the video clips which is extended to DOVER (Wu et al., 2023b) by incorporating aesthetics. SSL-VQA (Mitra & Soundararajan, 2024) learns a similar end-to-end model with limited labelled videos. KSVQE (Lu et al., 2024) employs CLIP (Radford et al., 2021) in its design while ModularVQA (Wen et al., 2024) also uses a CLIP model along with a spatial and temporal quality rectifier. However all these methods do not generalize well across diverse distortions.

To address generalizability, VISION (Mitra & Soundararajan, 2022), and CONVIQT (Madhusudana et al., 2022a) present self-supervised learning based quality-aware feature extractors. VQA methods such as STEM (Kancharla & Channappayya, 2022), VIQE (Zheng et al., 2022), VISION (Mitra & Soundararajan, 2022), and TPQI (Liao et al., 2022) do not require any human labelled videos in their design and give reasonable quality estimates for user-generated content (UGC) videos. Nevertheless, their performance with respect to the methods trained with human opinion scores is sub-par.

3 Quality Assessment using Latent Diffusion Models

We first discuss the preliminaries of latent diffusion models, followed by the procedure on how to adapt such models for IQA and VQA.

3.1 Preliminaries of Latent Diffusion Models

Latent diffusion models (LDMs) (Rombach et al., 2022) are a class of diffusion models that encode a real image x onto a low-dimensional latent space z and learn a distribution in the latent space conditioned on a text input y. In particular, the forward process starts at an image latent variable z_0 progressively corrupted by Gaussian noise, and a learned reverse process generates samples from the latent distribution using a denoising model conditioned on y. In LDMs, the image x is encoded as $z_0 = \varepsilon(x)$, where $\varepsilon(\cdot)$ is a vector quantized variational autoencoder (VQ-VAE). The generated latent samples are then passed through a decoder for image generation. Given any timestep t, the forward process distorts the latent representation z_0 to a noisy latent z_t as

$$z_t = \sqrt{\bar{\alpha}_t} z_0 + \sqrt{(1 - \bar{\alpha}_t)}\epsilon, \tag{1}$$

where $\epsilon \sim \mathcal{N}(0, \mathbf{I})$, $\bar{\alpha}_t = \prod_{s=1}^{t} \alpha_s$, $\alpha_t = 1 - \beta_t$ and $\{\beta\}_{t=1}^{T}$ are the noise variances at every timestep $t \in \{1, 2, \cdots, T\}$ in the forward process. In the reverse process, the denoising autoencoder $\epsilon_\theta(\cdot)$ takes in the noisy latent z_t, timestep variable t and the conditional variable y to estimate the additive noise in the forward process.

Given a text prompt y, let the CLIP text encoder output be $\tau_\theta(y) \in \mathbb{R}^{M \times d_\tau}$, where M is the number of text tokens and d_τ is the feature dimension. For a noisy latent z_t, let $\varphi_p(z_t) \in \mathbb{R}^{N^p \times d_\epsilon^p}$ be the intermediate (flattened) visual representation at block p, $p \in \{1, 2, \cdots, L\}$, in the denoiser UNet $\epsilon_\theta(\cdot)$, where N^p is the number of visual tokens. The intermediate cross-attention block of UNet maps the text representation onto the image representation for feature generation through the operation

$$\text{Attention}(Q^{(p)}, K^{(p)}, V^{(p)}) = \text{softmax}\left(\frac{Q^{(p)} {K^{(p)}}^T}{\sqrt{d}}\right) V^{(p)},$$

where $Q^{(p)} = W_Q^{(p)} \cdot \varphi_p(z_t)$, $K^{(p)} = W_K^{(p)} \cdot \tau_\theta(y)$ and $V^{(p)} = W_V^{(p)} \cdot \tau_\theta(y)$ are the query, key and value matrices with $W_Q^{(p)} \in \mathbb{R}^{d \times d_\epsilon^p}$, $W_K^{(p)} \in \mathbb{R}^{d \times d_\tau}$ and $W_V^{(p)} \in \mathbb{R}^{d \times d_\tau}$ being the respective projection matrices. d is a hyper-parameter corresponding to the number of channels in each head of the multi-head cross-attention. Note that, the dot operation shown above in the expression for $Q^{(p)}, K^{(p)}$, and $V^{(p)}$ is a linear operation and can be expanded as $Q^{(p)} = W_Q^{(p)} \cdot \varphi_p(z_t) = \varphi_p(z_t)(W_Q^{(p)})^T$ and similarly for $K^{(p)}$ and $V^{(p)}$.

3.2 Image Quality Assessment using LDM

Stable Diffusion model (SDM) Rombach et al. (2022) is trained with image-text pairs from LAION-5B Schuhmann et al. (2022) dataset. Such datasets include perceptual attributes in its prompts such as detailed descriptions that are related to visual quality, and aesthetic-style captioning. Moreover, the 5 billion dataset size encompasses diverse content and quality. While generating high-quality images from noisy latent features using text-guided prompts, the generative pipeline progressively retrieves perceptual attributes at various stages of the UNet. In this work, we seek to extract such intermediate generalized visual representations from UNet for the quality assessment task. To specifically retrieve quality-aware features, we rely upon using cross-attention block outputs, since textual representations can be leveraged to capture quality-specific information from the UNet. As argued by Kumari et. al. Kumari et al. (2023) , cross-attention parameters are more sensitive to finetuning of diffusion models over self-attention and other parameter weights.

Thus, our GenzIQA model exploits the generalization capabilities of the LDMs (Rombach et al., 2022) for IQA by learning cross-attention maps between the image and text features in the reverse diffusion process in conjunction with quality-aware prompts to match the visual concepts. In particular, we tap into the reverse diffusion process, where the UNet denoises noisy features as shown in Fig. 1. We train all the cross-attention modules in the denoising UNet of the LDM to output quality estimates at different scales. We use the LDM to obtain quality $q(x)$ for image x. Given the visual representation of image x at block p as $\varphi_p(z_t)$ and textual representation as $\tau_\theta(y)$, we compute the attention map at every block p of the UNet encoder and decoder as

$$A^{(p)} = \text{softmax}\left(\frac{Q^{(p)} {K^{(p)}}^T}{\sqrt{d}}\right), \tag{2}$$

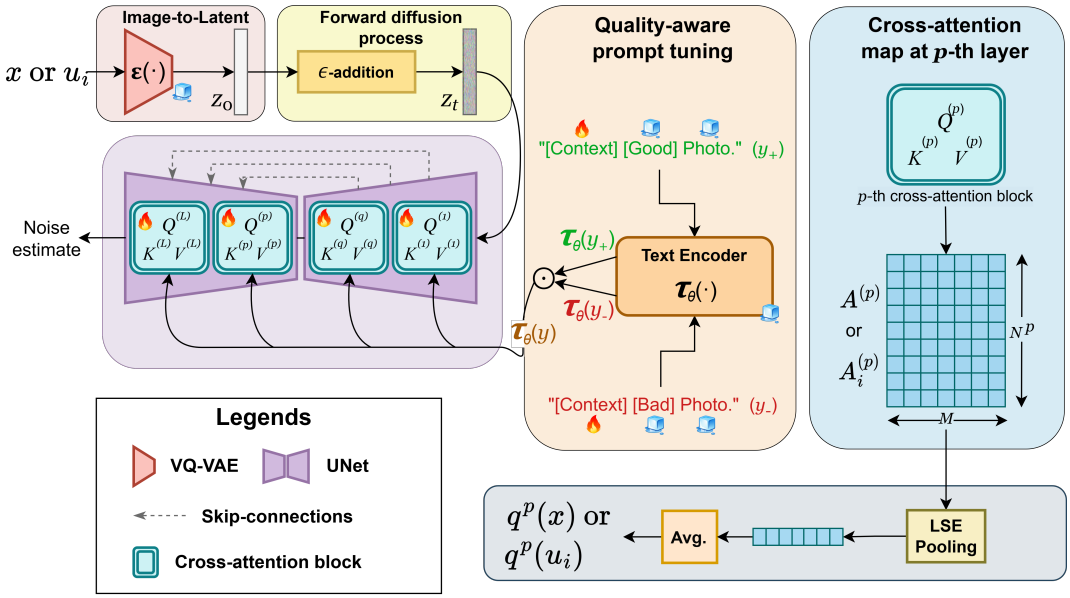

Figure 1: Given an input image x or video frame u_i, VQ-VAE processes it to the latent z_0. The noisy latent output z_t of the forward diffusion is fed to the denoising UNet (Ronneberger et al., 2015) $\epsilon_\theta(\cdot)$. At every cross-attention block in $\epsilon_\theta(\cdot)$, the intermediate visual representation is aligned with learnable text representations $\{\tau_\theta(y_+), \tau_\theta(y_-)\}$. After that, the attention maps are pooled for each cross-attention block p to predict block quality $q^p(x)$ or $q^p(u_i)$.

where $A^{(p)} \in \mathbb{R}^{N^p \times M}$ measures the similarity between the visual query at the pth block of the UNet and the textual embedding of the text encoder. In our framework, we only learn the cross-attention weights.

We estimate the image quality by applying a log-sum-exponential (LSE) pooling of the attention map at every scale leveraging upon its robustness benefits (He et al., 2023). The predicted quality of x at cross-attention block p is given as

$$q^p(x) = \frac{1}{M} \sum_{m=1}^{M} \frac{1}{\lambda} \log \left(\sum_{n=1}^{N^p} \exp(\lambda A_{n,m}^{(p)}) \right), \tag{3}$$

where $A_{n,m}^{(p)}$ is the attention score at location (n, m). λ is a temperature co-efficient used to amplify the similarity measure between the image and text features. The overall quality of image x is estimated as

$$q(x) = \frac{1}{L} \sum_{p=1}^{L} q^p(x). \tag{4}$$

We obtain $q(x)$ through a **single-step denoising** of z_t. The noise added to the latent features z_0, specified through t, can have a significant impact on the ability of the LDM to predict image quality. There is a delicate relationship between the denoising ability of the UNet and the amount of additive noise, which could alter the semantic information and image quality information in the latent image representation. We investigate this relationship in our experiments later.

We jointly optimize the projection matrices of the UNet ϵ_θ, and the prompt embedding layer of τ_θ using a mean squared error (MSE) loss between the ground-truth mean-opinion score (MOS), available in the training dataset and $q(x)$ as

$$\mathcal{L}_{\mathcal{IQA}} = ||q(x) - \text{MOS}(x)||_2^2. \tag{5}$$

Contextual Prompt Tuning: We further enhance the ability of the cross-attention maps to model quality through prompt-tuning. Prompt-tuning not only saves computational resources but also preserves the gen-

eralization capability of the text encoder. Similar to CLIP-IQA$^+$, we design a pair of context prompts with `'Good Photo'` and `'Bad Photo'` as the initial positive and negative attributes. Our final learnable context is given as

$$\begin{aligned} y_+ &= [Context] + \text{Positive Attribute} \quad \text{and} \\ y_- &= [Context] + \text{Negative Attribute}, \end{aligned} \tag{6}$$

where the $[Context]$ is a sequence of 16 tokens learned using CoOp (Zhou et al., 2022). Thus the text input y chosen for the IQA task is given by the pair $\{y_+, y_-\}$. We take the **average** of the two quality predictions corresponding to $\{y_+, y_-\}$, to estimate the final quality of the given image as we view the two quality predictions as estimates from two diverse quality-aware text prompts. Our initial (positive and negative) attributes give faster training convergence and also more accurate results rather than using only learnable contexts. While using a single prompt for representing quality, say `'Good Photo.'`, images with bad quality can manifest in various ways such as blurriness or compression or ringing artifacts. Such diverse notions of bad quality can make it challenging to align bad quality features together. Thus, specifying bad quality using an initial context such as `'Bad Photo.'`, helps to align all these different forms of highly distorted images into a unified representation. The same argument also applies to good quality features if only `'Bad Photo.'` is used as a single prompt.

3.3 Video Quality Assessment using LDM

Applying GenzIQA (using Stable Diffusion Model v2) on every video frame can take several minutes to process a 10-second long 1080p video clip on a NVIDIA RTX 3090 GPU. To alleviate the long inference time with respect to video duration, we estimate the video quality at 1 frame per second (fps) and then compensate for this subsampling.

Learning Sparse Video Quality: Consider a video clip $v = \{\bar{u}_j\}_{j=1}^{T_o}$, where $\bar{u}_j \in \mathbb{R}^{H\times W\times 3}$ is the jth frame of the video v and T_o is the total number of frames. We sub-sample the video v at one fps to get a sparse video clip $v_s = \{u_i\}_{i=1}^{T_s}$, where T_s is the number of frames of the sub-sampled video v_s and u_i is the ith sub-sampled frame. Given the visual representation of frame u_i at block p as $\varphi_p(z_t^i)$, we compute the attention map at every block p similar to GenzIQA as $A_i^{(p)} = \text{softmax}\left(\frac{Q_i^{(p)} {K_i^{(p)}}^T}{\sqrt{d}}\right)$. The predicted quality of v_s at cross-attention block p is given as $q^p(v_s) = \frac{1}{T_s}\sum_{i=1}^{T_s} q^p(u_i)$, where

$$q^p(u_i) = \frac{1}{M}\sum_{m=1}^{M}\frac{1}{\lambda}\log\left(\sum_{n=1}^{N^p}\exp(\lambda A_{i,n,m}^{(p)})\right), \tag{7}$$

and $A_{i,n,m}^{(p)}$ is the attention value at location (n, m) for the frame u_i. The overall quality of the sub-sampled video v_s is estimated as $q(v_s) = \frac{1}{L}\sum_{p=1}^{L} q^p(v_s)$.

Temporal Quality Modulator (TQM): Sub-sampling the video at one fps can lead to inaccurate estimation of the video quality (Wen et al., 2024). The temporal distortions pertaining to video motion cannot be accurately measured through a sparse sampling of the frames. Hence, we propose a TQM that fixes the quality estimate as shown in Fig. 2. Several recent works (Li et al., 2022; Sun et al., 2022; Wen et al., 2024) use the pre-trained SlowFast (Feichtenhofer et al., 2019) network to estimate motion-based quality in videos. The SlowFast network is a dual-stream model with a *Slow pathway*, operating at a low frame rate, and a *Fast pathway*, operating at a high frame rate. In our work, we utilize the slow and the fast pathways to estimate the video quality features at one fps and the actual frame rate, respectively. The SlowFast network is much smaller than the diffusion model and does not add much computational time.

We consider the SlowFast network that has been pre-trained on the video action recognition dataset viz. Kinetics-400K Kay et al. (2017). The slow pathway in SlowFast network is designed to capture spatial information in video frames from sub-sampled videos, while the fast pathway is designed to capture temporal information from the full-length video. As argued by Feichtenhofer et. al. Feichtenhofer et al. (2019), the fast pathway has better temporal modeling capability when compared to the slow pathway. Thus, we measure

the similarity of the visual query across all frames of v_s with the Slow and Fast pathway video features, respectively. We estimate how the similarities of the visual query across all frames of v_s with the slow features differ with its similarities of the fast features by passing both similarity scores through a network to obtain a scalar quality modulation factor.

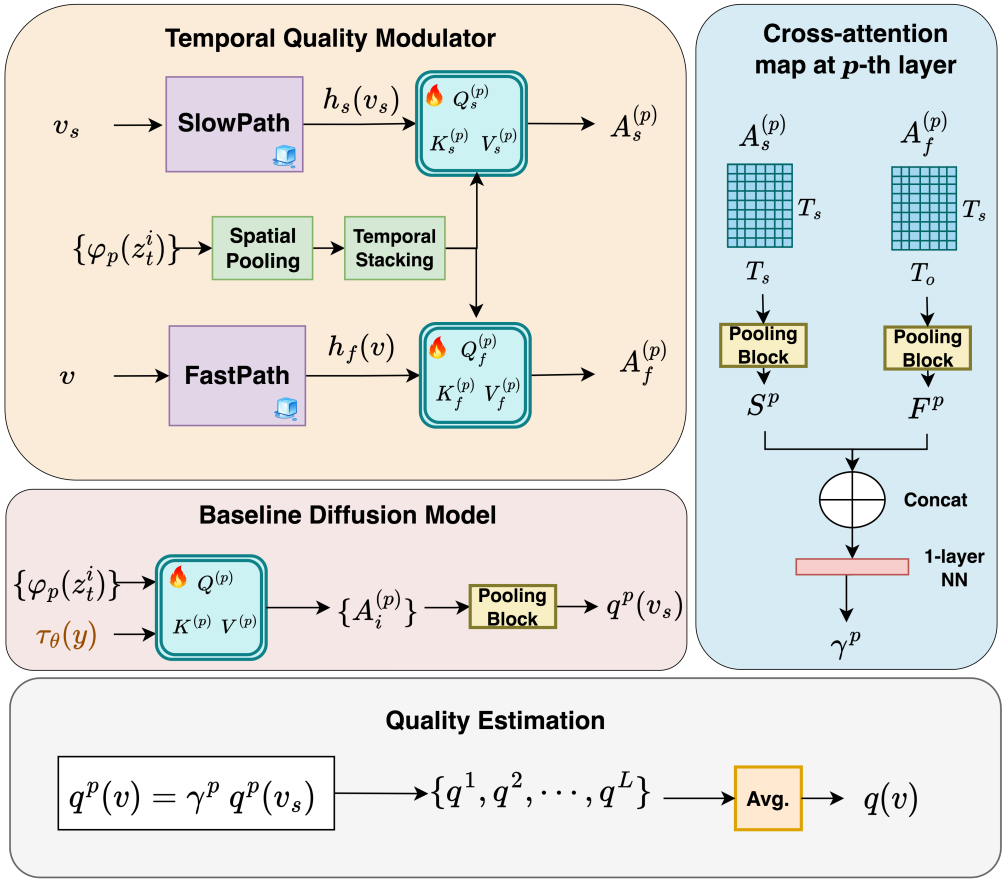

Figure 2: Framework of **Temporal Quality Modulator**. $\{\varphi_p(z_t^i)\}$ is the visual query feature of the UNet at the pth cross-attention block for a time-step t across all sub-sampled frames $i \in \{1, 2, \cdots, T_s\}$. Slow-pathway and fast-pathway features $h_s(v_s)$ and $h_f(v)$ are extracted from frozen slow and fast pathway of pre-trained SlowFastNet. Temporal correction factor γ_p is obtained by average pooling visual-motion cross-attention maps $A_s^{(p)}$ and $A_f^{(p)}$ across spatial dimension, then concatenating them and passing them through a single-layer neural network.

We extract the slow and fast pathway features from the pre-final layer of each pathway before each individual pathway's features are concatenated in the SlowFast network. Let $h_s(\cdot)$ and $h_f(\cdot)$ be the feature encoders for slow and fast pathways respectively. Then, the features corresponding to the sub-sampled and original videos are given as $h_s(v_s) \in \mathbb{R}^{T_s \times 256}$ and $h_f(v) \in \mathbb{R}^{T_o \times 2048}$. Let the query and key matrices at block p corresponding to the Slow pathway be $Q_s^{(p)}$ and $K_s^{(p)}$. Further, let $W_{sQ}^{(p)}$ and $W_{sK}^{(p)}$ be the corresponding weight matrices. Also, define frame-level quality $R_i^{(p)} = W_{sQ}^{(p)} \cdot \varphi_p(z_t^i)$ for $i \in \{1, 2, \cdots, T_s\}$. Thus, $R_i^{(p)} \in \mathbb{R}^{N^p \times d}$. We spatially average pool the frame-level queries along the visual-token dimension to obtain $Q_s^{(p)}$ as

$$Q_s^{(p)}(i, m) = \frac{1}{N^p} \sum_{n=1}^{N^p} R_{i,n,m}^{(p)}, \tag{8}$$

where $m \in \{1, 2, \cdots, d\}$. Therefore, $Q_s^{(p)} \in \mathbb{R}^{T_s \times d}$. Note that $K_s^{(p)} = W_{sK}^{(p)} \cdot h_s(v_s)$ and hence $K_s^{(p)} \in \mathbb{R}^{T_s \times d}$. Similarly, we get the query and key matrices at block p corresponding to the Fast features as $Q_f^{(p)} \in \mathbb{R}^{T_s \times d}$ and $K_f^{(p)} \in \mathbb{R}^{T_o \times d}$ with weight matrices $W_{fQ}^{(p)}$ and $W_{fK}^{(p)}$.

We get the attention maps between the denoising UNet and the SlowFast network features as $A_s^{(p)} = \text{softmax}\left(\frac{Q_s^{(p)} K_s^{(p)T}}{\sqrt{d}}\right)$ and $A_f^{(p)} = \text{softmax}\left(\frac{Q_f^{(p)} K_f^{(p)T}}{\sqrt{d}}\right)$, where $A_s^{(p)} \in \mathbb{R}^{T_s \times T_s}$ and $A_f^{(p)} \in \mathbb{R}^{T_s \times T_o}$ are the cross-attention maps with respect to the Slow and Fast pathway features respectively. We average pool the attention maps across spatial dimensions for all the cross-attention blocks $p \in \{1, 2, \ldots, L\}$ to get the cross-attention scores between the UNet feature and the SlowFast features as S^p and F^p. We concatenate the scores S^p and F^p and pass them through a single-layer network ϕ^p to get a temporal quality correction factor as $\gamma^p = \phi^p(S^p, F^p)$. We estimate the quality of the original video as

$$q(v) = \frac{1}{L} \sum_{p=1}^{L} \gamma^p q^p(v_s). \tag{9}$$

We optimize the projection matrices of the UNet ϵ_θ, the prompt embedding layer of τ_θ, TQM's cross-attention matrix weights $(W_{sQ}^{(p)}, W_{sK}^{(p)}, W_{fQ}^{(p)}, W_{fK}^{(p)})$ and ϕ^p for all p using MSE loss between the ground-truth MOS and $q(v)$ as

$$\mathcal{L}_{\mathcal{VQA}} = ||q(v) - \text{MOS}(v)||_2^2. \tag{10}$$

4 Experiments

4.1 Training Details:

We choose Stable Diffusion v2 (Rombach et al., 2022) model (SDM) pretrained on LAION-5B (Schuhmann et al., 2022) dataset with 1.45 billion parameters as our default LDM. We choose the model where the VQ-VAE (Razavi et al., 2019) takes in 512×512 image resolution. Thus, we resize the images and videos to 512×512 and process the images through the LDM. We freeze all parameters except the weight matrices of all the **16** cross-attention blocks in SDM-v2 as our goal is to adapt the cross-attention for the QA task. We train GenzIQA with MSE loss for 10 epochs with a batch size of 16 and Adam (Kingma & Ba, 2014) optimizer. We choose the timestep t in the range $(0-100]$, and $\lambda = 0.14$ as default based on 7K images of the official validation set of FLIVE (Ying et al., 2020b). Note that we refer to the noise variance in Eq. 1 through timestep t, implicitly referring to β_t. We train GenzVQA for 6 epochs using similar training parameters as GenzIQA. Since SDM is a T2I model, keeping the query weight frozen while learning GenzIQA is beneficial while for GenzVQA we train query weights along with key and value weights. (Analysis is given in Appendix A.2.)

During training, we randomly choose a **single timestep value** in the $(0-100]$ range for quality estimation. During inference, we chose a fixed timestep of 50 based on the GenzIQA's validation performance on official FLIVE Ying et al. (2020a) validation split. We experimented with other time-step values in the range $[10-90]$ and found that there is little variation in the validation performance. We evaluate both the models using the Spearman's Rank Order Correlation Co-efficient (SRCC) and the Pearson's Linear Correlation Co-efficient (PLCC) between the predicted quality and ground-truth human opinion scores. All experiments were conducted on a 24 GB NVIDIA RTX 3090 GPU with Pytorch 1.13.

4.2 Cross Database IQA Generalization

To study the generalizability of GenzIQA, we train it with the largest user generated content (UGC) dataset, specifically the official FLIVE (Ying et al., 2020a) train database comprising of 30,253 images, and test on diverse categories of distortions. In particular, we evaluate GenzIQA on various categories of test datasets such as **camera-captured** images (KonIQ-10K (Hosu et al., 2020), CLIVE (Ghadiyaram & Bovik, 2015)), **GAN-restored** images (PIPAL (Gu et al., 2020)), **night-time** images (NNID (Hu et al., 2021)), and

Table 1: Cross-database performance analysis of **GenzIQA** with other NR-IQA methods. All the methods are trained on **official FLIVE train** set and tested across various IQA databases. $*$ method does not have publicly available training code to benchmark on all databases. Bold and underlined numbers denote the best and second-best performance, respectively.

Methods	KonIQ-10K		CLIVE		PIPAL		NNID		CSIQ		LIVE-IQA		Average	
	SRCC	PLCC	SRCC	PLCC	SRCC	PLCC	SRCC	PLCC	SRCC	PLCC	SRCC	PLCC	SRCC	PLCC
TReS	0.669	0.710	0.729	0.714	0.362	0.359	0.805	0.794	0.587	0.517	0.543	0.445	0.612	0.589
HyperIQA	0.589	0.635	0.636	0.660	0.304	0.327	0.658	0.651	0.497	0.428	0.514	0.438	0.519	0.523
MetaIQA	0.578	0.489	0.448	0.410	0.340	0.312	0.452	0.429	0.562	0.536	0.732	0.673	0.486	0.479
MUSIQ	0.648	0.692	0.662	0.687	0.341	0.331	0.776	0.778	0.484	0.583	0.259	0.335	0.582	0.567
CLIP-IQA$^+$	0.724	0.756	0.657	0.673	0.271	0.293	0.694	0.702	0.591	0.617	0.611	0.617	0.592	0.609
Re-IQA	0.764	<u>0.787</u>	0.699	0.711	0.245	0.266	0.838	0.828	0.324	0.381	0.304	0.338	0.542	0.552
ARNIQA	0.766	0.768	0.707	0.729	0.362	0.373	0.782	0.762	0.482	0.508	0.498	0.485	0.601	0.604
GRepQ	**0.781**	0.786	0.736	0.753	0.303	0.318	<u>0.843</u>	<u>0.832</u>	0.579	0.587	0.666	0.568	0.638	0.641
QCN	0.732	0.783	0.724	<u>0.767</u>	<u>0.370</u>	<u>0.382</u>	0.814	0.808	<u>0.599</u>	<u>0.671</u>	**0.806**	**0.779**	<u>0.652</u>	<u>0.698</u>
DP-IQA*	0.771	-	0.770	-	-	-	-	-	-	-	-	-	-	-
PFD-IQA*	0.775	-	<u>0.783</u>	-	-	-	-	-	-	-	-	-	-	-
GenzIQA	<u>0.779</u>	**0.823**	**0.799**	**0.829**	**0.473**	**0.496**	**0.897**	**0.878**	**0.636**	**0.677**	<u>0.789</u>	<u>0.712</u>	**0.710**	**0.736**

Table 2: Cross-database performance analysis of **GenzVQA** with other NR-VQA methods on high frame-rate, Ultra-HD, gaming, and streaming videos. All methods are trained on **official LSVQ train** set. Bold and underline denote best and second best.

Methods	LIVE-YT-HFR		Waterloo-IVC-4K		LIVE-YT-Gaming		CGVDS		CSIQ-VQD		MD-VQA	
	SRCC	PLCC	SRCC	PLCC	SRCC	PLCC	SRCC	PLCC	SRCC	PLCC	SRCC	PLCC
VSFA	<u>0.461</u>	<u>0.528</u>	<u>0.465</u>	<u>0.487</u>	0.658	0.721	0.718	0.734	0.497	0.502	0.589	0.651
CSVT-BVQA	0.351	0.422	0.365	0.407	0.631	0.673	0.791	<u>0.811</u>	0.580	0.581	0.626	0.652
SimpleVQA	0.378	0.409	0.382	0.414	<u>0.666</u>	0.724	<u>0.804</u>	0.801	<u>0.599</u>	0.572	0.654	0.678
CONVIQT	0.321	0.403	0.358	0.385	0.572	0.618	0.791	<u>0.811</u>	0.580	0.581	0.633	0.665
DOVER	0.355	0.465	0.369	0.419	0.651	<u>0.730</u>	0.694	0.744	0.594	<u>0.598</u>	<u>0.708</u>	<u>0.690</u>
ModularVQA	0.350	0.427	0.404	0.456	**0.685**	**0.740**	0.722	0.775	0.520	0.524	0.588	0.617
GenzVQA	**0.644**	**0.662**	**0.493**	**0.562**	0.616	0.692	**0.822**	**0.839**	**0.694**	**0.707**	**0.724**	**0.721**

synthetically distorted images (CSIQ (Larson & Chandler, 2010) and LIVE-IQA (Sheikh et al., 2006)). We compare with popular state-of-the-art NR-IQA methods in literature such as TReS (Golestaneh et al., 2022), HyperIQA (Su et al., 2020), MetaIQA (Zhu et al., 2020), MUSIQ (Ke et al., 2021), CLIP-IQA$^+$ (Wang et al., 2023a), ARNIQA (Agnolucci et al., 2024), GRepQ (Srinath et al., 2024), Re-IQA (Saha et al., 2023), QCN (Shin et al., 2024), DP-IQA (Fu et al., 2024), and PFD-IQA Li et al. (2025). We note that all these methods are also trained on the official FLIVE train set for a fair comparison. CLIP-IQA$^+$ is an interesting comparison to GenzIQA as it is a vision-language model where learnable prompts are used to estimate quality from the visual and text features. Since LIQE (Zhang et al., 2023a), Q-Align (Wu et al., 2023d) requires detailed annotations of image-text context, we are not able to benchmark them due to the absence of such annotations on the FLIVE (Ying et al., 2020b) dataset. In Tab. 1, we compare with popular state-of-the-art NR-IQA methods in literature and observe that GenzIQA consistently outperforms other methods across various databases. Further, the performance on most databases is acceptable for IQA.

4.3 Cross Database VQA Generalization

We train GenzVQA with the largest UGC dataset, specifically, the official LSVQ (Ying et al., 2021) train database comprising 28,056 videos to evaluate its generalizabilty. In Tab. 2, we evaluate our model against domain-specific videos such as **frame-rate variation** (LIVE-YT-HFR (Madhusudana et al., 2021)), **Ultra-HD** (Waterloo-IVC-4K (Li et al., 2019b)), **gaming** (LIVE-YT-Gaming (Yu et al., 2022) and CGVDS (Zadtootaghaj et al., 2020)), and **streaming** (CSIQ-VQD (Vu & Chandler, 2014) and MD-VQA (Zhang et al., 2023c)) videos. In Tab. 3, we validate against popular VQA databases having **camera-captured** and **UGC** videos such as KoNViD-1K (Hosu et al., 2017), LIVE-VQC (Sinno & Bovik, 2019), Youtube-UGC (Wang et al., 2019), Maxwell (Wu et al., 2023c), and LIVE-Qualcomm (Ghadiyaram et al., 2018). We compare

Table 3: Cross-database performance analysis of **GenzVQA** with other NR-VQA methods on camera-captured and UGC videos. All methods are trained on **official LSVQ train** set. Average corresponds to the mean performance across all datasets in Tab. 2 and 3. Bold and underlined denote best and second best, respectively.

Methods	**LIVE-VQC**		**KoNViD-1K**		**Youtube-UGC**		**LIVE-Qualcomm**		**Maxwell**		**Average**	
	SRCC	PLCC	SRCC	PLCC	SRCC	PLCC	SRCC	PLCC	SRCC	PLCC	SRCC	PLCC
VSFA	0.753	0.795	0.810	0.811	0.718	0.721	0.438	0.434	0.649	0.654	0.614	0.639
CSVT-BVQA	0.793	0.811	0.843	0.835	0.802	0.792	0.520	0.568	0.594	0.588	0.627	0.649
SimpleVQA	0.749	0.789	0.826	0.820	0.802	0.806	0.570	0.617	0.697	0.704	0.647	0.667
CONVIQT	0.706	0.737	0.775	0.782	0.715	0.704	0.534	0.613	0.645	0.652	0.603	0.632
DOVER	**0.832**	**0.855**	0.884	0.883	0.777	0.792	0.668	0.704	0.728	0.730	0.660	0.691
ModularVQA	0.806	0.844	0.878	0.884	0.788	0.804	0.573	0.597	0.730	0.737	0.640	0.673
GenzVQA	0.826	0.840	**0.885**	**0.888**	**0.824**	**0.829**	**0.707**	**0.719**	**0.745**	**0.757**	**0.725**	**0.747**

GenzVQA with state-of-the-art VQA methods and see that our model achieves a consistently superior performance across various video content and distortions. In particular, our gains are substantial for high-frame rate VQA, showing the generalizability of GenzVQA.

We compare GenzVQA with only learning-based methods due to their superior performance with respect to the classical methods as noted in literature (Wu et al., 2023b; Lu et al., 2024). Due to the computational complexity of learning end-to-end VQA methods, earlier works such as VSFA (Li et al., 2019a), CSVT-BVQA (Li et al., 2022), SimpleVQA (Sun et al., 2022), and CONVIQT (Madhusudana et al., 2022a) only learn a regressor with pre-trained video representations. On the other hand, DOVER (Wu et al., 2023b) is an end-to-end VQA method. Since DOVER is an improved version of FAST-VQA (Wu et al., 2022), we do not compare with FAST-VQA. We also include a recent vision-language based VQA model viz. ModularVQA. We note that GenzVQA achieves a consistently superior performance against existing VQA methods across various video content and distortions. This experiment establishes the generalizability of GenzVQA against existing methods.

4.4 Ablation Studies and Detailed Experiments

4.4.1 Role of Noise in Latent Diffusion Model for Quality Estimation

The noise added to the latent features z_0 can have a significant impact on the ability of the latent diffusion model (LDM) to predict image or video frames' quality. Recall that the denoising UNet of LDM estimates the Gaussian noise incorporated in the forward process. We hypothesize that there is a delicate relationship between the denoising ability of the UNet and the amount of additive noise, which could alter the semantic information and quality information in the latent representation. We investigate this by gradually distorting the original image latent z_0 for a fixed length Markov chain. In particular, we generate the images using the pretrained Stable Diffusion v2 (Rombach et al., 2022) model as our default LDM (as mentioned in implementation details of main paper) with various noise steps in forward diffusion process.

In Fig. 3, we generate images from clean, low noise ($t = 95$) and high noise ($t = 950$) versions of the original image features. The generated image from the clean latent z_0 in Fig. 3b, is blurry as can be seen from the textureless outfield. This effect maybe attributed to the fact that denoising UNet removes bandpass texture information.

In Fig. 3d, we see that the addition of high Gaussian noise distorts the semantic information in the latent space and thus the UNet generates a content different from the original image. Finally, in Fig. 3c, the image generated preserves both the semantic and texture information as evident visually and from the respective LPIPS (Zhang et al., 2018a) scores. In our study, addition of the correct range of noise is extremely important as we wish to capture the perceptual and semantic information at all intermediate stages of the UNet.

(a) Reference Image (b) LPIPS:**0.1537** (c) LPIPS:**0.1023** (d) LPIPS:**0.5287**

Figure 3: Generated images from zero shot SDM. In Fig. 3b image is generated without noise infused to the image latent, Fig. 3c and Fig. 3d are generated images with noise fed at the timestep $t = 95$ (low noise), and $t = 950$ (high noise) respectively and subsequently denoised. Lower LPIPS scores correspond to better perceptual quality.

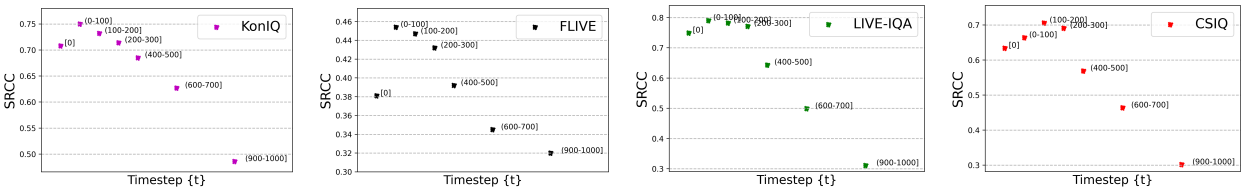

Figure 4: SRCC performance variation of GenzIQA trained on **CLIVE** and tested across four databases at different timesteps.

4.4.2 Impact of Noise Level Variation

The level of noise added to the image latent space has a direct impact on the ability of the denoiser to preserve perceptual information. Thus, we train GenzIQA on the CLIVE database with varying levels of noise added to the input. Specifically, we train on CLIVE and test on various dataset for a single-timestep sampled in the range $\{0, (0-100], (100-200], (200-300], (400-500], (600-700], (900-1000]\}$. As evident from Fig. 4, the performance across various test datasets is fairly consistent in the range $(0-300]$, while it starts to drastically degrade for noisy timesteps beyond 400. We conclude that corrupting the image latent with high noise distorts the semantic information, thus hindering the extraction of quality relevant information from the cross-attention map. Further, extremely low noise levels cause blur during denoising, leading to poorer quality prediction performance. We see that sampling a single-timestep from the $(0, 100]$ range offers a reasonable performance across all datasets.

4.4.3 Impact of major components of GenzIQA

We evaluate the need of cross-attention finetuning between images and textual prompts, learning quality-aware prompts, and LSE pooling (versus average pooling). In Tab. 4, we train GenzIQA on CLIVE and test on KonIQ_{test}, FLIVE_{test}, NNID, and LIVE-IQA. The zero-shot performance reported in the first row indicates that all components of GenzIQA are necessary to adapt LDM for IQA. Learning the cross-attention map has the maximum impact on performance. However, prompt tuning and LSE pooling also lead to consistent improvements across databases.

4.4.4 Impact of major components of GenzVQA

We perform experiments in Tab. 5 with respect to GenzVQA. We first observe that training the baseline diffusion model on a VQA dataset such as LSVQ gives a significant improvement over training it on an IQA dataset such as FLIVE.

Table 4: Impact of various components of **GenzIQA** trained on **CLIVE** and tested on four datasets. We report the SRCC performance.

Prompt Tuning	Vision -Text Cross-Attn.	LSE Pool	Test Data			
			KonIQ test	FLIVE test	NNID	LIVE-IQA
×	×	×	0.184	0.010	0.032	0.124
✓	×	✓	0.455	0.284	0.517	0.636
×	✓	✓	0.696	0.331	0.677	0.706
✓	✓	×	0.735	0.438	0.721	0.773
✓	✓	✓	**0.750**	**0.454**	**0.738**	**0.782**

Table 5: Impact of various components of GenzVQA evaluated on four datasets. We report the SRCC performance.

Train Data	SlowFast Feature	Vision-Motion Cross-Attn.	Test Data			
			YT-UGC	LIVE-VQC	YT-HFR	CSIQ-VQD
FLIVE	×	×	0.495	0.673	0.358	0.394
LSVQ	×	×	0.806	0.768	0.494	0.583
LSVQ	✓	×	0.809	0.775	0.538	0.666
LSVQ	✓	✓	**0.824**	**0.826**	**0.644**	**0.694**

a) Impact of SlowFast features: One of GenzVQA's main components is the temporal quality modulator. Recent works such as CSVT-BVQA, SimpleVQA, and ModularVQA use pre-trained SlowFast features and regress directly against quality. Thus, we replace our TQM with a two-layer neural network that regresses SlowFast features directly to get the temporal quality correction factor. We notice a gain in performance while using the SlowFast features along with the baseline diffusion model.

b) Impact of Vision-Motion Cross-Attention module: A significant gain in performance is observed with the inclusion of the cross-attention module in TQM with respect to the baseline model across all datasets. In particular, cross-attention between the SlowFast motion features and the UNet visual features is advantageous over merely using SlowFast features. This experiment establishes the importance of learning shared information between the UNet and SlowFast networks for TQM.

4.4.5 Impact of VAE on Distortions

Our GenzIQA's backbone viz. SDM applies a diffusion model on the latent space of VQ-VAE. In this experiment, we analyze the impact of both image resizing and VQ-VAE on the image/ video frame distortions. In particular, we show the 2D tSNE (Tu et al., 2021b) visualization of the cross-attention representations averaged across all blocks of the UNet model. In Figure 5, we show the features for (a) JPEG compression, (b) white noise, and (c) Gaussian blur images from LIVE-IQA belonging to high MOS (> 70) and low MOS(< 40). We infer that for all distortion types, the diffusion features can segregate images based on their distortion levels. Thus, we observe the distortion information is reasonably preserved despite the resizing and use of VQ-VAE for effective quality assessment.

4.4.6 Impact of Slow and Fast Attention Module

In Table 6, we compare the prediction accuracy given by GenzVQA for two videos. For Video 1, the baseline prediction without any fast and slow cross-attention is much lesser than the actual ground-truth. The baseline prediction gets amplified by the ratio of fast to slow cross-attention score to GenzVQA's prediction. Note that we compute fast and slow cross-attention at every scale of Stable diffusion's UNet and get the

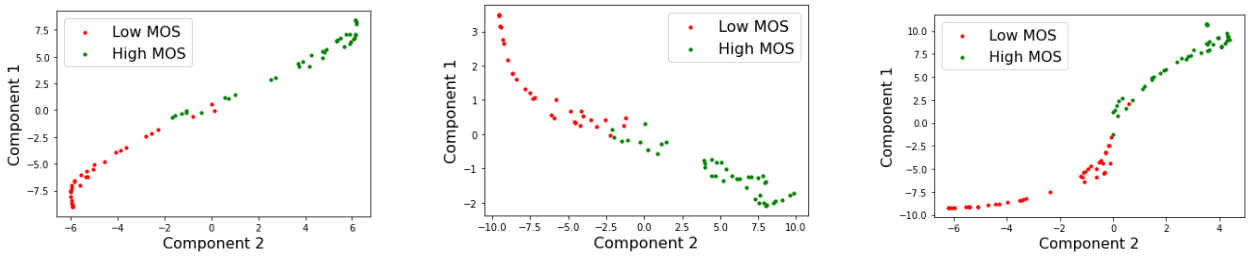

(a) Blur (b) Noise (c) Compression

Figure 5: 2D tSNE visualization of cross-attention features of GenzIQA trained on FLIVE and tested on (a) Gaussian blur, (b) White noise, and (c) JPEG compressed images from LIVE-IQA.

Table 6: Performance comparison of GenzVQA with and without Fast and Slow cross-attention blocks. Video 1 and 2 are selected from LIVE-VQC (Sinno & Bovik, 2019) dataset.

	Video 1	Video 2
MOS	85.207	18.616
Baseline	56.894	52.153
Mean Fast Score	1.22	0.9136
Mean Slow Score	0.9312	1.3798
GenzVQA	75.225	36.9243

GenzVQA prediction as an average over all scales as given in Equation 9 in main paper. But for ease of understanding here, we provide the average of fast and slow cross-attention scores across all scales. Similarly, for Video 2, the baseline prediction is much higher than ground-truth. Thus, the baseline gets dampened by the ratio of fast and slow cross-attentions scores.

4.4.7 Intra-database Performance

a) Intra-database Performance of GenzIQA: We now validate the performance of our model in intra-database train-test settings. Specifically, we train GenzIQA with either the official train set or 80% of image samples from various databases and test on the official test set or remaining 20%, respectively. In Tab. 7, in case of FLIVE and KonIQ-10K, we train-test on the official split provided, while for other datasets, we randomly split the data 10 times in the ratio 80 : 20 and report the median performance. We compare GenzIQA with other NR-IQA methods in the same setting. We also benchmark LIQE (Zhang et al., 2023a) by training it on individual datasets (wherever detailed text annotation was provided). We infer that our method gives competitive performance with recent state-of-the-art methods across all databases. We conclude from Tab. 7 that GenzIQA not only outperforms recent benchmarks in practical cross/inter database generalization scenarios but also does remarkably well on intra-database test scenarios.

b) Transfer Learning GenzVQA on Smaller Datasets: Similar to other works such as FAST-VQA (Wu et al., 2022), DOVER (Wu et al., 2023b), and ModularVQA (Wen et al., 2024), we finetune GenzVQA on individual evaluation datasets viz. LIVE-VQC (Sinno & Bovik, 2019), KoNViD-1K (Hosu et al., 2017), and Youtube-UGC (Wang et al., 2019), LIVE-Qualcomm (Ghadiyaram et al., 2018) and LIVE-YT-Gaming

Table 7: Performance comparison of **GenzIQA** with other NR-IQA methods on Intra-database setting. All results are obtained from from their respective publications.

Methods	FLIVE		KonIQ-10K		CLIVE		LIVE-IQA		SPAQ		CSIQ	
	SRCC	PLCC	SRCC	PLCC	SRCC	PLCC	SRCC	PLCC	SRCC	PLCC	SRCC	PLCC
TReS	0.554	0.625	0.915	0.928	0.846	0.877	0.969	0.968	-	-	0.922	0.942
HyperIQA	0.535	0.623	0.906	0.917	0.859	0.882	0.962	0.966	0.916	0.919	0.923	0.942
DB-CNN	0.554	0.652	0.875	0.884	0.851	0.869	0.968	0.971	0.911	0.915	0.946	0.959
CONTRIQUE	0.580	0.651	0.894	0.904	0.845	0.857	0.960	0.961	0.914	0.919	0.942	0.955
Re-IQA	0.645	0.733	0.914	0.923	0.840	0.854	0.970	0.971	0.918	0.925	0.947	0.960
LIQE	-	-	0.918	0.908	0.889	0.879	0.958	0.942	-	-	0.923	0.918
ARNIQA	0.595	0.671	-	-	-	-	0.966	0.970	0.905	0.910	0.962	0.973
GRepQ	0.531	0.582	0.908	0.916	0.859	0.867	0.945	0.943	0.874	0.877	0.948	0.955
QPT	0.645	0.733	0.927	0.941	**0.895**	**0.914**	-	-	0.925	0.928	-	-
QCN	0.644	**0.741**	0.934	0.945	0.875	0.893	-	-	0.923	0.928	-	-
LoDA	0.578	0.679	0.932	0.944	0.876	0.899	**0.975**	**0.979**	0.925	0.928	-	-
DSMix	**0.646**	**0.735**	0.915	0.925	0.873	0.883	0.974	0.974	-	-	0.957	0.962
GenzIQA	0.627	0.728	**0.936**	**0.950**	0.879	0.897	0.966	0.968	**0.929**	**0.935**	**0.968**	**0.972**

Table 8: Finetune performance comparison of **GenzVQA** with other NR-VQA methods on various databases. KSVQE results are from (Lu et al., 2024) and all other methods numbers are taken from ModularVQA.

Methods	LSVQ-test		LSVQ-1080p		LIVE-VQC		KoNViD-1K		Youtube-UGC		LIVE-Qualcomm		LIVE-YT-Gaming	
	SRCC	PLCC	SRCC	PLCC	SRCC	PLCC	SRCC	PLCC	SRCC	PLCC	SRCC	PLCC	SRCC	PLCC
VSFA	0.801	0.796	0.675	0.704	0.718	0.771	0.794	0.799	0.787	0.789	0.708	0.774	0.784	0.819
CSVT-BVQA	0.852	0.854	0.772	0.788	0.841	0.839	0.839	0.830	0.825	0.818	0.833	0.837	0.852	0.868
SimpleVQA	0.866	0.863	0.750	0.793	0.740	0.775	0.792	0.798	0.819	0.817	0.722	0.774	0.814	0.836
FastVQA	0.876	0.877	0.779	0.814	0.853	0.873	0.893	0.887	0.863	0.859	0.807	0.814	0.869	0.880
DOVER	0.888	0.889	0.795	0.830	0.853	0.872	0.892	0.900	0.875	0.874	0.736	0.789	0.882	0.906
ModularVQA	0.895	0.895	0.809	0.844	0.860	0.880	0.901	0.905	0.876	0.877	0.832	0.842	0.867	0.902
KSVQE	0.886	0.888	0.790	0.823	0.861	0.883	**0.922**	**0.921**	0.900	0.912	-	-	-	-
GenzVQA	**0.898**	**0.899**	**0.797**	**0.835**	**0.871**	**0.882**	0.909	0.918	**0.910**	**0.913**	**0.851**	**0.856**	**0.878**	**0.907**

(Yu et al., 2022) in 80 : 20 train-test ratio for 10 splits and report the median performance. In case of LSVQ (Ying et al., 2021), we train on the official train split and report the performances on the official test and 1080p splits. We compare GenzVQA with other popular NR-VQA in Tab. 8. We infer that GenzVQA outperforms the state-of-the art methods on most databases.

4.4.8 Analyzing Cross-Attention Map Representation

We visualize the cross-attention representation of GenzIQA trained on FLIVE to understand why it leads to superior generalization. For this, we subsample good and bad quality images from three different test datasets with MOS less than 30 and greater than 70, respectively. In Fig. 6, we show the 2D tSNE (Tu et al., 2021b) visualization of the cross-attention map in Eq. (2) averaged across all blocks, timestep samples and the number of image tokens. In particular, we chose a perplexity of 40 and iterated the optimization over 1000 steps while generating the tSNE plot. We conclude that the learned attention representation clearly separates high and low-quality images as evident from Fig. 6. Under similar settings, we also visualize the representation of CLIP-IQA$^+$ visual encoder conditioned on the same prompt pair attributes. In particular, the visual feature similarity with ensemble text representation gives a 2-dimensional representation for each image. We see that the CLIP-IQA$^+$ model's separability is somewhat inferior to what we see with the cross-attention features of GenzIQA.

4.4.9 Analysis of Contextual Prompt Learning

a) Study on Learnable Prompt vs Fixed Prompt:

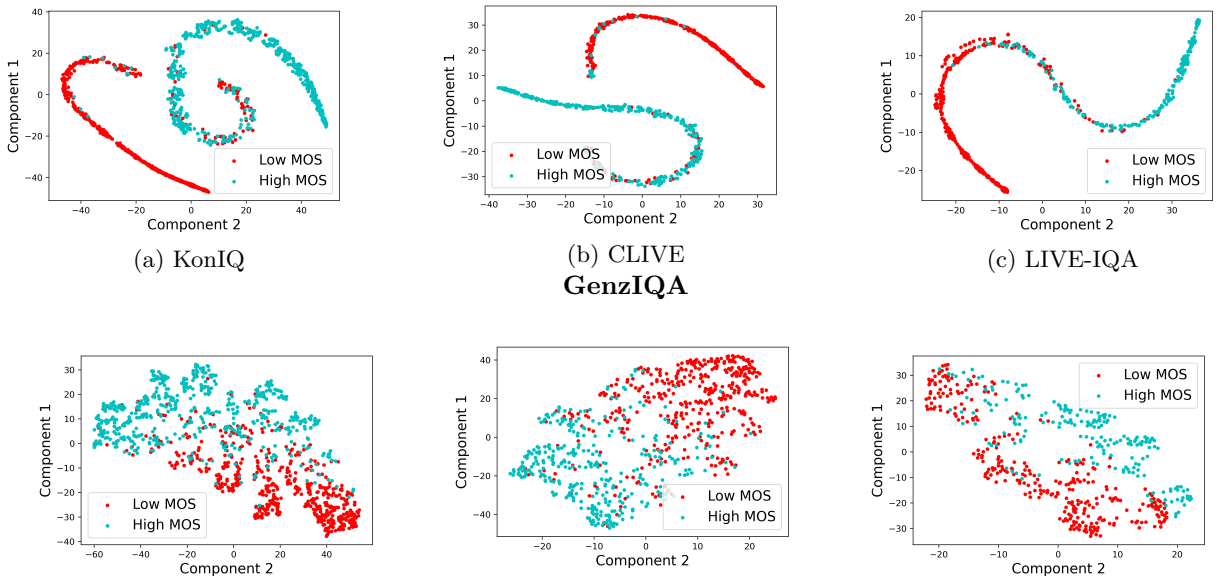

(a) KonIQ (b) CLIVE (c) LIVE-IQA

GenzIQA

(d) KonIQ (e) CLIVE (f) LIVE-IQA

CLIP-IQA$^+$

Figure 6: 2D tSNE visualization of cross-attention features of **GenzIQA** trained on **FLIVE** and tested on images from KonIQ, CLIVE, and LIVE-IQA. CLIP-IQA$^+$ similarity features conditioned on antonym prompts are also shown.

GenzIQA and GenzVQA by default are trained with learnable antonym prompts using CoOp (Zhou et al., 2022) similar to CLIP-IQA$^+$. We study the need for diverse prompts pairs as well as the need for learnable context vectors vs fixed prompts in case of GenzIQA. In Tab. 9, we choose *['Good Photo.', 'Bad Photo.']* as the initial antonym prompt pair while for the single prompt case, we only choose *['Good Photo.']*. We make two observations from this study. Firstly, antonym prompt pairs give a better performance than a single prompt in both the learnable prompt and fixed prompt training across all test datasets. Secondly, learnable prompts consistently yield superior results with respect to the fixed prompt case. Both these phenomena are expected as multiple studies show the benefit of prompt learning (Yao et al., 2023; Guo et al., 2023; Wang et al., 2023a).

Table 9: SRCC performance variation of **GenzIQA** on the choice of prompts being fed as input to the CLIP text encoder. All the variations have been trained on **FLIVE** official train set and cross-tested on these datasets. **Good Photo / Bad Photo** as initial attributes.

Test database	Trainable single prompt	Trainable antonym prompts	Fixed single prompt	Fixed antonym prompts
CLIVE	0.791	0.799	0.784	0.789
NNID	0.880	0.897	0.871	0.874
CSIQ	0.622	0.636	0.568	0.611
LIVE-IQA	0.783	0.789	0.731	0.759

b) Analysis on Choice of Prompts: In our experimental studies, we choose *['Good Photo.', 'Bad Photo.']* as our initial learnable antonym prompt attributes. As shown in CLIP-IQA$^+$ (Wang et al., 2023a), this prompt pair gives the best estimate of quality. Here, we train GenzIQA with the official FLIVE training set for initial prompts *['High Quality.', 'Low Quality.']* in Tab. 10, and *['High Definition.', 'Low Definition.']* in

Table 10: SRCC performance variation of **GenzIQA** trained on FLIVE with **High Quality / Low Quality** as initial prompts.

Test database	**Trainable single prompt**	**Trainable antonym prompts**	**Fixed single prompt**	**Fixed antonym prompts**
CLIVE	0.776	0.795	0.758	0.761
NNID	0.883	0.889	0.870	0.872
CSIQ	0.616	0.623	0.546	0.576
LIVE-IQA	0.782	0.812	0.734	0.742

Table 11: SRCC performance variation of **GenzIQA** trained on FLIVE with **High Definition / Low Definition** as initial prompts.

Test database	**Trainable single prompt**	**Trainable antonym prompts**	**Fixed single prompt**	**Fixed antonym prompts**
CLIVE	0.768	0.791	0.752	0.755
NNID	0.880	0.892	0.869	0.871
CSIQ	0.612	0.620	0.548	0.564
LIVE-IQA	0.780	0.800	0.728	0.738

Tab. 11 under different settings. We see that there is minimal variation in performance with respect to the exact choice of these popular quality relevant antonym prompt attributes.

4.5 Run Time:

The average test-time required by GenzIQA to estimate quality for a single 512×512 resized image for one timestep on a 24 GB NVIDIA RTX 3090 is **0.035** seconds. While for a 8-second long 30 fps video, GenzVQA takes **0.357** seconds to estimate quality. Similar to FastVQA (Wu et al., 2022) and ModularVQA (Wen et al., 2024), we infer GenzVQA for 8 second long 30 fps 1080p videos on an NVIDIA RTX 3090 GPU. We compare the inference time of GenzVQA with other NR-VQA methods in Tab. 12. We note that inference time of GenzVQA (0.357 secs) is much lesser than actual duration (8 secs) of the video. We also compare the number of model parameter of GenzVQA with other VQA methods. Even though the number of parameters of GenzVQA is higher than other benchmarking methods, applying the T2I diffusion model at 1 fps keeps the latency during training/ inference within comparable limits.

Table 12: Inference time and Model parameters comparison of GenzVQA with other NR-VQA methods for 8 second long 30 fps 1080p videos.

Method	Inference Time(sec)	Parameters(millions)
VSFA	11.109	24.1
CSVT-BVQA	27.632	58.6
SimpleVQA	0.714	58.3
FastVQA	0.045	28.1
DOVER	0.047	56.2
ModularVQA	0.159	87.8
GenzVQA	0.357	950

5 Conclusion

In this work, we presented GenzIQA and GenzVQA by leveraging the benefits of LDM. Our work is perhaps one of the earliest attempts at understanding whether and how such models can be used for generalized

NR-IQA and NR-VQA. In this context, it is important to finetune the cross-attention module and learn quality-aware input context vectors to enable the diffusion models be effective for QA. Also, we introduce a cost-effective way to estimate video quality by introducing our TQM. Although our method can be readily deployed on servers or on the cloud, the complexity of a large vision language model can limit its deployment on edge devices. It would be interesting to explore knowledge distillation (Meng et al., 2023) and inference-time acceleration techniques Salimans & Ho (2022) for edge-deployment of GenzIQA and GenzVQA. On the other hand, while GenzIQA achieves very good performance on most datasets, there is still scope for improvement on PIPAL, which requires a more fine-grained approach to IQA. Nevertheless, we believe that GenzIQA and GenzVQA will encourage further studies on the use of generative models for superior and practical QA.

References

Lorenzo Agnolucci, Leonardo Galteri, Marco Bertini, and Alberto Del Bimbo. Arniqa: Learning distortion manifold for image quality assessment. In *Proceedings of the IEEE/CVF Winter Conference on Applications of Computer Vision*, pp. 189–198, 2024.

Yuming Fang, Hanwei Zhu, Yan Zeng, Kede Ma, and Zhou Wang. Perceptual quality assessment of smartphone photography. In *Proceedings of the IEEE/CVF Conference on Computer Vision and Pattern Recognition*, pp. 3677–3686, 2020.

Christoph Feichtenhofer, Haoqi Fan, Jitendra Malik, and Kaiming He. Slowfast networks for video recognition. In *Proceedings of the IEEE/CVF international conference on computer vision*, pp. 6202–6211, 2019.

Honghao Fu, Yufei Wang, Wenhan Yang, and Bihan Wen. Dp-iqa: Utilizing diffusion prior for blind image quality assessment in the wild. *arXiv preprint arXiv:2405.19996*, 2024.

Deepti Ghadiyaram and Alan C Bovik. Massive online crowdsourced study of subjective and objective picture quality. *IEEE Transactions on Image Processing*, 25(1):372–387, 2015.

Deepti Ghadiyaram, Janice Pan, Alan C. Bovik, Anush Krishna Moorthy, Prasanjit Panda, and Kai-Chieh Yang. In-capture mobile video distortions: A study of subjective behavior and objective algorithms. *IEEE Transactions on Circuits and Systems for Video Technology*, 28(9):2061–2077, 2018. doi: 10.1109/TCSVT.2017.2707479.

S Alireza Golestaneh, Saba Dadsetan, and Kris M Kitani. No-reference image quality assessment via transformers, relative ranking, and self-consistency. In *Proceedings of the IEEE/CVF Winter Conference on Applications of Computer Vision*, pp. 1220–1230, 2022.

Jinjin Gu, Haoming Cai, Haoyu Chen, Xiaoxing Ye, Jimmy Ren, and Chao Dong. Pipal: a large-scale image quality assessment dataset for perceptual image restoration. In *European Conference on Computer Vision (ECCV) 2020*, pp. 633–651. Springer International Publishing, 2020.

Jiayi Guo, Chaofei Wang, You Wu, Eric Zhang, Kai Wang, Xingqian Xu, Shiji Song, Humphrey Shi, and Gao Huang. Zero-shot generative model adaptation via image-specific prompt learning. In *Proceedings of the IEEE/CVF Conference on Computer Vision and Pattern Recognition (CVPR)*, pp. 11494–11503, June 2023.

Kaiming He, Xiangyu Zhang, Shaoqing Ren, and Jian Sun. Deep residual learning for image recognition. In *Proceedings of the IEEE conference on Computer Vision and Pattern Recognition*, pp. 770–778, 2016.

Xuehai He, Weixi Feng, Tsu-Jui Fu, Varun Jampani, Arjun Akula, Pradyumna Narayana, Sugato Basu, William Yang Wang, and Xin Eric Wang. Discriminative diffusion models as few-shot vision and language learners. *arXiv preprint arXiv:2305.10722*, 2023.

Vlad Hosu, Franz Hahn, Mohsen Jenadeleh, Hanhe Lin, Hui Men, Tamás Szirányi, Shujun Li, and Dietmar Saupe. The konstanz natural video database (konvid-1k). In *2017 Ninth International Conference on Quality of Multimedia Experience (QoMEX)*, pp. 1–6. IEEE, 2017.

Vlad Hosu, Hanhe Lin, Tamas Sziranyi, and Dietmar Saupe. Koniq-10k: An ecologically valid database for deep learning of blind image quality assessment. *IEEE Transactions on Image Processing*, 29:4041–4056, 2020.

Runze Hu, Yutao Liu, Zhanyu Wang, and Xiu Li. Blind quality assessment of night-time image. *Displays*, 69:102045, 2021.

Zahra Kadkhodaie, Florentin Guth, Eero P Simoncelli, and Stéphane Mallat. Generalization in diffusion models arises from geometry-adaptive harmonic representation. In *12th ICLR*, 2024.

Parimala Kancharla and Sumohana S. Channappayya. Completely blind quality assessment of user generated video content. *IEEE Transactions on Image Processing*, 31:263–274, 2022. doi: 10.1109/TIP.2021.3130541.

Bahjat Kawar, Shiran Zada, Oran Lang, Omer Tov, Huiwen Chang, Tali Dekel, Inbar Mosseri, and Michal Irani. Imagic: Text-based real image editing with diffusion models. In *Proceedings of the IEEE/CVF Conference on Computer Vision and Pattern Recognition*, pp. 6007–6017, 2023.

Will Kay, Joao Carreira, Karen Simonyan, Brian Zhang, Chloe Hillier, Sudheendra Vijayanarasimhan, Fabio Viola, Tim Green, Trevor Back, Paul Natsev, et al. The kinetics human action video dataset. *arXiv preprint arXiv:1705.06950*, 2017.

Junjie Ke, Qifei Wang, Yilin Wang, Peyman Milanfar, and Feng Yang. Musiq: Multi-scale image quality transformer. In *Proceedings of the IEEE/CVF International Conference on Computer Vision*, pp. 5148–5157, 2021.

Jongyoo Kim and Sanghoon Lee. Fully deep blind image quality predictor. *IEEE Journal of selected topics in signal processing*, 11(1):206–220, 2016.

Diederik P Kingma and Jimmy Ba. Adam: A method for stochastic optimization. *arXiv preprint arXiv:1412.6980*, 2014.

J. Korhonen. Two-level approach for no-reference consumer video quality assessment. *IEEE Transactions on Image Processing*, 28(12):5923–5938, 2019.

Nupur Kumari, Bingliang Zhang, Richard Zhang, Eli Shechtman, and Jun-Yan Zhu. Multi-concept customization of text-to-image diffusion. In *Proceedings of the IEEE/CVF conference on computer vision and pattern recognition*, pp. 1931–1941, 2023.

Eric C Larson and Damon M Chandler. Most apparent distortion: full-reference image quality assessment and the role of strategy. *Journal of Electronic Imaging*, 19(1):011006–011006, 2010.

Alexander C Li, Mihir Prabhudesai, Shivam Duggal, Ellis Brown, and Deepak Pathak. Your diffusion model is secretly a zero-shot classifier. *arXiv preprint arXiv:2303.16203*, 2023a.

Bowen Li, Weixia Zhang, Meng Tian, Guangtao Zhai, and Xianpei Wang. Blindly assess quality of in-the-wild videos via quality-aware pre-training and motion perception. *IEEE Transactions on Circuits and Systems for Video Technology*, 32(9):5944–5958, 2022.

Chunyi Li, Zicheng Zhang, Haoning Wu, Wei Sun, Xiongkuo Min, Xiaohong Liu, Guangtao Zhai, and Weisi Lin. Agiqa-3k: An open database for ai-generated image quality assessment. *arXiv preprint arXiv:2306.04717*, 2023b.

Chunyi Li, Tengchuan Kou, Yixuan Gao, Yuqin Cao, Wei Sun, Zicheng Zhang, Yingjie Zhou, Zhichao Zhang, Weixia Zhang, Haoning Wu, Xiaohong Liu, Xiongkuo Min, and Guangtao Zhai. Aigiqa-20k: A large database for ai-generated image quality assessment. In *2024 IEEE/CVF Conference on Computer Vision and Pattern Recognition Workshops (CVPRW)*, pp. 6327–6336, 2024a. doi: 10.1109/CVPRW63382.2024.00636.

Dingquan Li, Tingting Jiang, and Ming Jiang. Quality assessment of in-the-wild videos. MM '19, pp. 2351–2359, New York, NY, USA, 2019a. Association for Computing Machinery. ISBN 9781450368896. doi: 10.1145/3343031.3351028. URL https://doi.org/10.1145/3343031.3351028.

Dingquan Li, Tingting Jiang, and Ming Jiang. Unified quality assessment of in-the-wild videos with mixed datasets training. *International Journal of Computer Vision*, 129(4):1238–1257, Apr 2021. ISSN 1573-1405. doi: 10.1007/s11263-020-01408-w. URL https://doi.org/10.1007/s11263-020-01408-w.

Xudong Li, Jingyuan Zheng, Runze Hu, Yan Zhang, Ke Li, Yunhang Shen, Xiawu Zheng, Yutao Liu, ShengChuan Zhang, Pingyang Dai, et al. Feature denoising diffusion model for blind image quality assessment. *arXiv preprint arXiv:2401.11949*, 2024b.

Xudong Li, Yan Zhang, Yunhang Shen, Ke Li, Runze Hu, Xiawu Zheng, and Sicheng Zhao. Feature denoising diffusion model for blind image quality assessment. In *Proceedings of the AAAI Conference on Artificial Intelligence*, volume 39, pp. 5004–5012, 2025.

Zhuoran Li, Zhengfang Duanmu, Wentao Liu, and Zhou Wang. Avc, hevc, vp9, avs2 or av1? — a comparative study of state-of-the-art video encoders on 4k videos. In *Image Analysis and Recognition: 16th International Conference, ICIAR 2019, Waterloo, ON, Canada, August 27–29, 2019, Proceedings, Part I*, pp. 162–173, Berlin, Heidelberg, 2019b. Springer-Verlag. ISBN 978-3-030-27201-2. doi: 10.1007/978-3-030-27202-9_14. URL https://doi.org/10.1007/978-3-030-27202-9_14.

Liang Liao, Kangmin Xu, Haoning Wu, Chaofeng Chen, Wenxiu Sun, Qiong Yan, and Weisi Lin. Exploring the effectiveness of video perceptual representation in blind video quality assessment. MM '22, pp. 837–846, New York, NY, USA, 2022. Association for Computing Machinery. ISBN 9781450392037. doi: 10.1145/3503161.3547849. URL https://doi.org/10.1145/3503161.3547849.

Hanhe Lin, Vlad Hosu, and Dietmar Saupe. Kadid-10k: A large-scale artificially distorted iqa database. In *2019 Eleventh International Conference on Quality of Multimedia Experience (QoMEX)*, pp. 1–3, 2019. doi: 10.1109/QoMEX.2019.8743252.

Yiting Lu, Xin Li, Yajing Pei, Kun Yuan, Qizhi Xie, Yunpeng Qu, Ming Sun, Chao Zhou, and Zhibo Chen. Kvq: Kwai video quality assessment for short-form videos. In *Proceedings of the IEEE/CVF Conference on Computer Vision and Pattern Recognition (CVPR)*, pp. 25963–25973, June 2024.

Chaofan Ma, Yuhuan Yang, Chen Ju, Fei Zhang, Jinxiang Liu, Yu Wang, Ya Zhang, and Yanfeng Wang. Diffusionseg: Adapting diffusion towards unsupervised object discovery. *arXiv preprint arXiv:2303.09813*, 2023.

Pavan C Madhusudana, Xiangxu Yu, Neil Birkbeck, Yilin Wang, Balu Adsumilli, and Alan C Bovik. Subjective and objective quality assessment of high frame rate videos. *IEEE Access*, 9:108069–108082, 2021.

Pavan C. Madhusudana, Neil Birkbeck, Yilin Wang, Balu Adsumilli, and Alan C. Bovik. Conviqt: Contrastive video quality estimator, 2022a. URL https://arxiv.org/abs/2206.14713.

Pavan C Madhusudana, Neil Birkbeck, Yilin Wang, Balu Adsumilli, and Alan C Bovik. Image quality assessment using contrastive learning. *IEEE Transactions on Image Processing*, 31:4149–4161, 2022b.

Chenlin Meng, Robin Rombach, Ruiqi Gao, Diederik Kingma, Stefano Ermon, Jonathan Ho, and Tim Salimans. On distillation of guided diffusion models. In *Proceedings of the IEEE/CVF Conference on Computer Vision and Pattern Recognition*, pp. 14297–14306, 2023.

Shankhanil Mitra and Rajiv Soundararajan. Multiview contrastive learning for completely blind video quality assessment of user generated content. In *Proceedings of the 30th ACM International Conference on Multimedia*, MM '22, pp. 1914–1924, New York, NY, USA, 2022. Association for Computing Machinery. ISBN 9781450392037. doi: 10.1145/3503161.3548064. URL https://doi.org/10.1145/3503161.3548064.

Shankhanil Mitra and Rajiv Soundararajan. Knowledge guided semi-supervised learning for quality assessment of user generated videos. In *Proceedings of the AAAI Conference on Artificial Intelligence*, volume 38, pp. 4251–4260, 2024.

Anish Mittal, Anush Krishna Moorthy, and Alan Conrad Bovik. No-reference image quality assessment in the spatial domain. *IEEE Transactions on Image Processing*, 21(12):4695–4708, 2012.

Anush Krishna Moorthy and Alan Conrad Bovik. Blind image quality assessment: From natural scene statistics to perceptual quality. *IEEE Transactions on Image Processing*, 20(12):3350–3364, 2011.

Fei Peng, Huiyuan Fu, Anlong Ming, Chuanming Wang, Huadong Ma, Shuai He, Zifei Dou, and Shu Chen. Aigc image quality assessment via image-prompt correspondence. In *2024 IEEE/CVF Conference on Computer Vision and Pattern Recognition Workshops (CVPRW)*, pp. 6432–6441, 2024. doi: 10.1109/CVPRW63382.2024.00644.

Nikolay Ponomarenko, Lina Jin, Oleg Ieremeiev, Vladimir Lukin, Karen Egiazarian, Jaakko Astola, Benoit Vozel, Kacem Chehdi, Marco Carli, Federica Battisti, and C.-C. Jay Kuo. Image database tid2013: Peculiarities, results and perspectives. *Signal Processing: Image Communication*, 30:57–77, 2015. ISSN 0923-5965. doi: https://doi.org/10.1016/j.image.2014.10.009. URL `https://www.sciencedirect.com/science/article/pii/S0923596514001490`.

Guanyi Qin, Runze Hu, Yutao Liu, Xiawu Zheng, Haotian Liu, Xiu Li, and Yan Zhang. Data-efficient image quality assessment with attention-panel decoder. In *Proceedings of the AAAI Conference on Artificial Intelligence (AAAI)*, 2023.

Alec Radford, Jong Wook Kim, Chris Hallacy, Aditya Ramesh, Gabriel Goh, Sandhini Agarwal, Girish Sastry, Amanda Askell, Pamela Mishkin, Jack Clark, et al. Learning transferable visual models from natural language supervision. In *International Conference on Machine Learning*, pp. 8748–8763. PMLR, 2021.

R. Rassool. VMAF reproducibility: Validating a perceptual practical video quality metric. In *2017 IEEE International Symposium on Broadband Multimedia Systems and Broadcasting (BMSB)*, pp. 1–2, 2017.

Ali Razavi, Aaron Van den Oord, and Oriol Vinyals. Generating diverse high-fidelity images with vq-vae-2. *Advances in neural information processing systems*, 32, 2019.

Robin Rombach, Andreas Blattmann, Dominik Lorenz, Patrick Esser, and Björn Ommer. High-resolution image synthesis with latent diffusion models. In *Proceedings of the IEEE/CVF conference on computer vision and pattern recognition*, pp. 10684–10695, 2022.

Olaf Ronneberger, Philipp Fischer, and Thomas Brox. U-net: Convolutional networks for biomedical image segmentation. In *Medical Image Computing and Computer-Assisted Intervention–MICCAI 2015: 18th International Conference, Munich, Germany, October 5-9, 2015, Proceedings, Part III 18*, pp. 234–241. Springer, 2015.

Subhadeep Roy, Shankhanil Mitra, Soma Biswas, and Rajiv Soundararajan. Test time adaptation for blind image quality assessment. In *Proceedings of the IEEE/CVF International Conference on Computer Vision*, pp. 16742–16751, 2023.

Michele A Saad, Alan C Bovik, and Christophe Charrier. Blind image quality assessment: A natural scene statistics approach in the dct domain. *IEEE Transactions on Image Processing*, 21(8):3339–3352, 2012.

Michele A Saad, Alan C Bovik, and Christophe Charrier. Blind prediction of natural video quality. *IEEE Transactions on Image Processing*, 23(3):1352–1365, 2014.

Avinab Saha, Sandeep Mishra, and Alan C. Bovik. Re-iqa: Unsupervised learning for image quality assessment in the wild. In *Proceedings of the IEEE/CVF Conference on Computer Vision and Pattern Recognition (CVPR)*, pp. 5846–5855, June 2023.

Tim Salimans and Jonathan Ho. Progressive distillation for fast sampling of diffusion models. *arXiv preprint arXiv:2202.00512*, 2022.

Christoph Schuhmann, Romain Beaumont, Richard Vencu, Cade Gordon, Ross Wightman, Mehdi Cherti, Theo Coombes, Aarush Katta, Clayton Mullis, Mitchell Wortsman, et al. Laion-5b: An open large-scale dataset for training next generation image-text models. *Advances in Neural Information Processing Systems*, 35:25278–25294, 2022.

H.R. Sheikh, M.F. Sabir, and A.C. Bovik. A statistical evaluation of recent full reference image quality assessment algorithms. *IEEE Transactions on Image Processing*, 15(11):3440–3451, 2006. doi: 10.1109/TIP.2006.881959.

Jinsong Shi, Pan Gao, Xiaojiang Peng, and Jie Qin. Dsmix: Distortion-induced sensitivity map based pre-training for no-reference image quality assessment, 2024. URL `https://arxiv.org/abs/2407.03886`.

Nyeong-Ho Shin, Seon-Ho Lee, and Chang-Su Kim. Blind image quality assessment based on geometric order learning. In *2024 IEEE/CVF Conference on Computer Vision and Pattern Recognition (CVPR)*, pp. 12799–12808, 2024. doi: 10.1109/CVPR52733.2024.01216.

Zeina Sinno and Alan C Bovik. Large-scale study of perceptual video quality. *IEEE Transactions on Image Processing*, 28(2):612–627, 2019.

R. Soundararajan and A. C. Bovik. Rred indices: Reduced reference entropic differencing framework for image quality assessment. In *2011 IEEE International Conference on Acoustics, Speech and Signal Processing (ICASSP)*, pp. 1149–1152, 2011.

Rajiv Soundararajan and Alan C Bovik. Video quality assessment by reduced reference spatio-temporal entropic differencing. *IEEE Transactions on Circuits and Systems for Video Technology*, 23(4):684–694, 2013.

Suhas Srinath, Shankhanil Mitra, Shika Rao, and Rajiv Soundararajan. Learning generalizable perceptual representations for data-efficient no-reference image quality assessment. In *Proceedings of the IEEE/CVF Winter Conference on Applications of Computer Vision*, pp. 22–31, 2024.

Shaolin Su, Qingsen Yan, Yu Zhu, Cheng Zhang, Xin Ge, Jinqiu Sun, and Yanning Zhang. Blindly assess image quality in the wild guided by a self-adaptive hyper network. In *Proceedings of the IEEE/CVF Conference on Computer Vision and Pattern Recognition*, pp. 3667–3676, 2020.

Wei Sun, Xiongkuo Min, Wei Lu, and Guangtao Zhai. A deep learning based no-reference quality assessment model for ugc videos. In *Proceedings of the 30th ACM International Conference on Multimedia*, pp. 856–865, 2022.

Zhengzhong Tu, Yilin Wang, Neil Birkbeck, Balu Adsumilli, and Alan C. Bovik. Ugc-vqa: Benchmarking blind video quality assessment for user generated content. *IEEE Transactions on Image Processing*, 30: 4449–4464, 2021a. doi: 10.1109/TIP.2021.3072221.

Zhengzhong Tu, Xiangxu Yu, Yilin Wang, Neil Birkbeck, Balu Adsumilli, and Alan C Bovik. Rapique: Rapid and accurate video quality prediction of user generated content. *IEEE Open Journal of Signal Processing*, 2:425–440, 2021b.

Phong V. Vu and Damon M. Chandler. ViS3: an algorithm for video quality assessment via analysis of spatial and spatiotemporal slices. *Journal of Electronic Imaging*, 23(1):1 – 25, 2014. doi: 10.1117/1.JEI.23.1.013016. URL `https://doi.org/10.1117/1.JEI.23.1.013016`.

Jianyi Wang, Kelvin C.K. Chan, and Chen Change Loy. Exploring clip for assessing the look and feel of images. In *Proceedings of the Thirty-Seventh AAAI Conference on Artificial Intelligence*, AAAI'23. AAAI Press, 2023a. ISBN 978-1-57735-880-0. doi: 10.1609/aaai.v37i2.25353. URL `https://doi.org/10.1609/aaai.v37i2.25353`.

Jiarui Wang, Huiyu Duan, Jing Liu, Shi Chen, Xiongkuo Min, and Guangtao Zhai. Aigciqa2023: A large-scale image quality assessment database for ai generated images: from the perspectives of quality, authenticity and correspondence. In *CAAI International Conference on Artificial Intelligence*, pp. 46–57. Springer, 2023b.

Yilin Wang, Sasi Inguva, and Balu Adsumilli. Youtube ugc dataset for video compression research. In *2019 IEEE 21st International Workshop on Multimedia Signal Processing (MMSP)*, pp. 1–5, 2019. doi: 10.1109/MMSP.2019.8901772.

Zhaoyang Wang, Bo Hu, Mingyang Zhang, Jie Li, Leida Li, Maoguo Gong, and Xinbo Gao. Diffusion model-based visual compensation guidance and visual difference analysis for no-reference image quality assessment. *IEEE Transactions on Image Processing*, 2025.

Zhou Wang, Alan C Bovik, Hamid R Sheikh, and Eero P Simoncelli. Image quality assessment: from error visibility to structural similarity. *IEEE Transactions on Image Processing*, 13(4):600–612, 2004.

Wen Wen, Mu Li, Yabin Zhang, Yiting Liao, Junlin Li, Li Zhang, and Kede Ma. Modular Blind Video Quality Assessment . In *2024 IEEE/CVF Conference on Computer Vision and Pattern Recognition (CVPR)*, pp. 2763–2772, Los Alamitos, CA, USA, June 2024. IEEE Computer Society. doi: 10.1109/CVPR52733.2024.00267. URL `https://doi.ieeecomputersociety.org/10.1109/CVPR52733.2024.00267`.

Haoning Wu, Chaofeng Chen, Jingwen Hou, Liang Liao, Annan Wang, Wenxiu Sun, Qiong Yan, and Weisi Lin. Fast-vqa: Efficient end-to-end video quality assessment with fragment sampling. In Shai Avidan, Gabriel Brostow, Moustapha Cissé, Giovanni Maria Farinella, and Tal Hassner (eds.), *Computer Vision – ECCV 2022*, pp. 538–554, Cham, 2022. Springer Nature Switzerland. ISBN 978-3-031-20068-7.

Haoning Wu, Liang Liao, Jingwen Hou, Chaofeng Chen, Erli Zhang, Annan Wang, Wenxiu Sun, Qiong Yan, and Weisi Lin. Exploring opinion-unaware video quality assessment with semantic affinity criterion. *IEEE International Conference on Multimedia and Expo (ICME)*, 2023a.

Haoning Wu, Erli Zhang, Liang Liao, Chaofeng Chen, Jingwen Hou, Annan Wang, Wenxiu Sun, Qiong Yan, and Weisi Lin. Exploring video quality assessment on user generated contents from aesthetic and technical perspectives. In *Proceedings of the IEEE/CVF International Conference on Computer Vision (ICCV)*, pp. 20144–20154, October 2023b.

Haoning Wu, Erli Zhang, Liang Liao, Chaofeng Chen, Jingwen Hou, Annan Wang, Wenxiu Sun, Qiong Yan, and Weisi Lin. Towards explainable in-the-wild video quality assessment: a database and a language-prompted approach. *arXiv preprint arXiv:2305.12726*, 2023c.

Haoning Wu, Zicheng Zhang, Weixia Zhang, Chaofeng Chen, Chunyi Li, Liang Liao, Annan Wang, Erli Zhang, Wenxiu Sun, Qiong Yan, Xiongkuo Min, Guangtao Zhai, and Weisi Lin. Q-align: Teaching lmms for visual scoring via discrete text-defined levels. *arXiv preprint arXiv:2312.17090*, 2023d. Equal Contribution by Wu, Haoning and Zhang, Zicheng. Corresponding Authors: Zhai, Guangtao and Lin, Weisi.

J. Xu, P. Ye, Y. Liu, and D. Doermann. No-reference video quality assessment via feature learning. In *2014 IEEE International Conference on Image Processing (ICIP)*, pp. 491–495, 2014. doi: 10.1109/ICIP.2014.7025098.

Jingtao Xu, Peng Ye, Qiaohong Li, Haiqing Du, Yong Liu, and David Doermann. Blind image quality assessment based on high order statistics aggregation. *IEEE Transactions on Image Processing*, 25(9): 4444–4457, 2016. doi: 10.1109/TIP.2016.2585880.

Kangmin Xu, Liang Liao, Jing Xiao, Chaofeng Chen, Haoning Wu, Qiong Yan, and Weisi Lin. Boosting image quality assessment through efficient transformer adaptation with local feature enhancement. In *2024 IEEE/CVF Conference on Computer Vision and Pattern Recognition (CVPR)*, pp. 2662–2672, 2024. doi: 10.1109/CVPR52733.2024.00257.

Hantao Yao, Rui Zhang, and Changsheng Xu. Visual-language prompt tuning with knowledge-guided context optimization. In *Proceedings of the IEEE/CVF Conference on Computer Vision and Pattern Recognition (CVPR)*, pp. 6757–6767, June 2023.

Peng Ye, Jayant Kumar, Le Kang, and David Doermann. Unsupervised feature learning framework for no-reference image quality assessment. In *2012 IEEE conference on Computer Vision and Pattern Recognition*, pp. 1098–1105. IEEE, 2012.

Z. Ying, H. Niu, P. Gupta, D. Mahajan, D. Ghadiyaram, and A. Bovik. From patches to pictures (paq-2-piq): Mapping the perceptual space of picture quality. In *2020 IEEE/CVF Conference on Computer Vision and Pattern Recognition (CVPR)*, pp. 3572–3582, Los Alamitos, CA, USA, jun 2020a. IEEE Computer Society. doi: 10.1109/CVPR42600.2020.00363. URL https://doi.ieeecomputersociety.org/10.1109/CVPR42600.2020.00363.

Zhenqiang Ying, Haoran Niu, Praful Gupta, Dhruv Mahajan, Deepti Ghadiyaram, and Alan Bovik. From patches to pictures (paq-2-piq): Mapping the perceptual space of picture quality. In *Proceedings of the IEEE/CVF Conference on Computer Vision and Pattern Recognition*, pp. 3575–3585, 2020b.

Zhenqiang Ying, Maniratnam Mandal, Deepti Ghadiyaram, and Alan Bovik. Patch-vq: 'patching up' the video quality problem. In *Proceedings of the IEEE/CVF Conference on Computer Vision and Pattern Recognition (CVPR)*, pp. 14019–14029, June 2021.

Xiangxu Yu, Zhengzhong Tu, Zhenqiang Ying, Alan C Bovik, Neil Birkbeck, Yilin Wang, and Balu Adsumilli. Subjective quality assessment of user-generated content gaming videos. In *Proceedings of the IEEE/CVF Winter Conference on Applications of Computer Vision*, pp. 74–83, 2022.

Saman Zadtootaghaj, Steven Schmidt, Saeed Shafiee Sabet, Sebastian Möller, and Carsten Griwodz. Quality estimation models for gaming video streaming services using perceptual video quality dimensions. In *Proceedings of the 11th ACM Multimedia Systems Conference*, MMSys '20, pp. 213–224, New York, NY, USA, 2020. Association for Computing Machinery. ISBN 9781450368452. doi: 10.1145/3339825.3391872. URL https://doi.org/10.1145/3339825.3391872.

Hui Zeng, Lei Zhang, and Alan C. Bovik. A probabilistic quality representation approach to deep blind image quality prediction. *CoRR*, abs/1708.08190, 2017. URL http://arxiv.org/abs/1708.08190.

Richard Zhang, Phillip Isola, Alexei A Efros, Eli Shechtman, and Oliver Wang. The unreasonable effectiveness of deep features as a perceptual metric. In *Proceedings of the IEEE conference on Computer Vision and Pattern Recognition*, pp. 586–595, 2018a.

Richard Zhang, Phillip Isola, Alexei A Efros, Eli Shechtman, and Oliver Wang. The unreasonable effectiveness of deep features as a perceptual metric. In *Proceedings of the IEEE conference on computer vision and pattern recognition*, pp. 586–595, 2018b.

Weixia Zhang, Kede Ma, Jia Yan, Dexiang Deng, and Zhou Wang. Blind image quality assessment using a deep bilinear convolutional neural network. *IEEE Transactions on Circuits and Systems for Video Technology*, 30(1):36–47, 2018c.

Weixia Zhang, Guangtao Zhai, Ying Wei, Xiaokang Yang, and Kede Ma. Blind image quality assessment via vision-language correspondence: A multitask learning perspective. In *Proceedings of the IEEE/CVF Conference on Computer Vision and Pattern Recognition*, pp. 14071–14081, 2023a.

Zicheng Zhang, Chunyi Li, Wei Sun, Xiaohong Liu, Xiongkuo Min, and Guangtao Zhai. A perceptual quality assessment exploration for aigc images. *arXiv e-prints*, pp. arXiv–2303, 2023b.

Zicheng Zhang, Wei Wu, Wei Sun, Danyang Tu, Wei Lu, Xiongkuo Min, Ying Chen, and Guangtao Zhai. Md-vqa: Multi-dimensional quality assessment for ugc live videos. In *Proceedings of the IEEE/CVF Conference on Computer Vision and Pattern Recognition*, pp. 1746–1755, 2023c.

Kai Zhao, Kun Yuan, Ming Sun, Mading Li, and Xing Wen. Quality-aware pre-trained models for blind image quality assessment. In *Proceedings of the IEEE/CVF Conference on Computer Vision and Pattern Recognition*, pp. 22302–22313, 2023.

Qi Zheng, Zhengzhong Tu, Xiaoyang Zeng, Alan C. Bovik, and Yibo Fan. A completely blind video quality evaluator. *IEEE Signal Processing Letters*, 29:2228–2232, 2022. doi: 10.1109/LSP.2022.3215311.

Kaiyang Zhou, Jingkang Yang, Chen Change Loy, and Ziwei Liu. Learning to prompt for vision-language models. *International Journal of Computer Vision*, 130(9):2337–2348, 2022.

Hancheng Zhu, Leida Li, Jinjian Wu, Weisheng Dong, and Guangming Shi. Metaiqa: Deep meta-learning for no-reference image quality assessment. In *Proceedings of the IEEE/CVF Conference on Computer Vision and Pattern Recognition*, pp. 14143–14152, 2020.

A Appendix

A.1 Impact of Denoising Steps on Quality Estimation

In Fig.3 of the main paper, we showed that a moderate noise variance is effective while extracting quality features during a single denoising step of reverse diffusion. We now address the complementary question of whether increasing the number of denoising steps and using the latent features from the output after more denoising steps can yield richer features. To understand this, we conduct an experiment where we let $t \in (0, 100]$ and increase the number of denoising steps from 1 to 5 by reducing t by 20 in each successive step. This reduction of t aligns with how LDM suggests what noise needs to be added in successive denoising steps. We train the **GenzIQA** model on the CLIVE dataset and test on multiple datasets for this experiment. In Tab. 13, we observe that the multi-step denoising performance is always inferior to the single-step denoising performance, and the performance degrades as we tap features from successive denoisers. We believe that since the cross-attention matrices are tuned for quality estimation, this can impact the ability of the denoiser to remove noise for its effective use in successive steps of multi-step denoising. We conclude that it is best to use a single step denoiser to extract quality-aware features from diffusion models.

Table 13: SRCC performance variation of GenzIQA in several steps of a multistep denoising process.

Test database	**1st denoising step**	**3rd denoising step**	**5th denoising step**
KonIQ_{test}	0.747	0.631	0.562
LIVE-IQA	0.782	0.638	0.476
NNID	0.737	0.557	0.417
CSIQ	0.661	0.496	0.415

A.2 Impact of Vision-Language Cross-Attention Components

In implementation details, we kept the weight matrix $W_Q^{(p)}$ of the query for all cross-attention blocks $p \in \{1, 2, \cdots, L\}$ frozen for **GenzIQA** as we want to preserve the robust visual information captured by the pre-trained text-to image (T2I) Stable diffusion model (SDM). The key and value weights are obtained based on the text prompt, the context of which is also learnt. Thus, we update the key and value weights. In this section, we analyze the impact of freezing query, key and value weights on quality estimation. In Tab. 14, we evaluate GenzIQA trained on CLIVE against four different IQA databases viz. the official test set of KonIQ-10K (Hosu et al., 2020), FLIVE (Ying et al., 2020a) and entire NNID (Hu et al., 2021), and LIVE-IQA (Sheikh et al., 2006). We infer from the last row that making query weights trainable has an adverse impact on performance. Similarly, freezing the key and value weights also affects the performance.

In case of **GenzVQA**, since SDM is a T2I model, we find that learning the query weights (in addition to key and value weights like GenzIQA) is beneficial, as seen in Tab. 15. We infer that learning the query weights is important in capturing spatial attributes in the video which are absent in image representations of the pre-trained T2I model.

A.3 Choice of Sampling Timesteps

In the implementation details of the main paper, we chose a single sampling timesteps during testing for both GenzIQA and GenzVQA. In Fig. 7, we evaluate GenzIQA trained on the official FLIVE (Ying et al., 2020b) training set on KonIQ (Hosu et al., 2020), CLIVE (Ghadiyaram & Bovik, 2015), NNID (Hu et al., 2021), and LIVE-IQA (Sheikh et al., 2006) with respect to the number of sampling steps. We see that as the number of sampling steps during evaluation increases, the performance also marginally increases and saturates at around 4 on all datasets. Thus, we chose a single sampling timestep for faster test-time evaluations.

Table 14: SRCC performance analysis on the impact of various components of Cross-Attention block in GenzIQA trained on **CLIVE** and tested on four datasets.

Query Weights	Key Weights	Value Weights	KonIQ_{test}	FLIVE_{test}	NNID	LIVE-IQA
×	×	×	0.455	0.284	0.517	0.636
✓	×	×	0.715	0.410	0.713	0.657
×	✓	✓	**0.750**	**0.454**	**0.738**	**0.782**
✓	✓	✓	**0.750**	0.426	0.718	0.752

Table 15: SRCC performance analysis on the impact of learning query in GenzVQA trained on the official LSVQ training set and evaluated on seven datasets. Key and value are trainable in both the instances.

Query Weights	LIVE-VQC	KoNVid-1K	YT-UGC	LIVE-QCOMM	Waterloo-4K	YT-Gaming	CSIQ-VQD
×	0.810	0.874	0.814	0.680	0.453	0.598	0.678
✓	**0.826**	**0.885**	**0.824**	**0.707**	**0.493**	**0.616**	**0.694**

A.4 Comparison of GenzIQA and LIQE

LIQE (Zhang et al., 2023a) extends CLIP-IQA$^+$ and has shown very promising performance. However it requires detailed text annotations in the form of quality, distortion and scene information for training. Since FLIVE (Ying et al., 2020a) does not have such detailed annotations, we were unable to benchmark it in Tab. 1. Thus, for a fair comparison with LIQE (Zhang et al., 2023a), we train GenzIQA **solely** on the combination of KADID-10K (Lin et al., 2019) and KonIQ-10K (similar to Table 2 of LIQE). We evaluate GenzIQA and LIQE on various IQA datasets such as TID (Ponomarenko et al., 2015), SPAQ (Fang et al., 2020), PIPAL (Gu et al., 2020), CLIVE (Ghadiyaram & Bovik, 2015), LIVE-IQA (Sheikh et al., 2006) (denoted as LIVE) and NNID (Hu et al., 2021) in a cross-dataset generalized setting and present the SRCC performance in Tab. 16. We note that GenzIQA does better than LIQE in most datasets despite not requiring any detailed text annotations.

A.5 Cross-Database Generalization on AI Generated Images

In this section, we investigate the effectiveness of our approach in cross-database generalization on the AI-Generated Image (AIGI) databases. To explore this, we choose the largest AIGI database currently available, AIGIQA-20K (Li et al., 2024a) and train GenzIQA on it. The official train split is available for the AIGIQA-

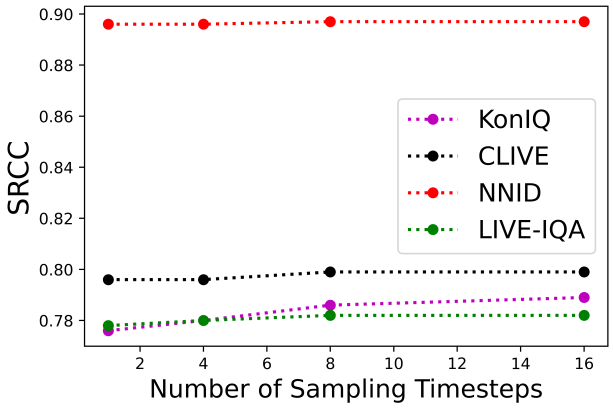

Figure 7: Performance analysis of GenzIQA with varying number of sampling timesteps during evaluation across four test databases.

Table 16: SRCC performance comparison of GenzIQA with LIQE trained on KADID-10K and KonIQ-10K and evaluated across multiple datasets.

Method	TID	SPAQ	PIPAL	CLIVE	LIVE	NNID
LIQE	0.811	0.881	0.478	0.830	**0.868**	0.785
GenzIQA	**0.820**	**0.892**	**0.486**	**0.860**	0.847	**0.797**

Table 17: SRCC performance comparison of GenzIQA with other state-of-the-art NR-IQA methods in a cross-database scenario on AI-generated image databases. All models are trained on AIGIQA-20K (Li et al., 2024a), the cross-database evaluation is done for other 3 databases.

Methods	AGIQA-3K		AGIQA-1K		AIGCIQA2023	
	SRCC	PLCC	SRCC	PLCC	SRCC	PLCC
CLIP-IQA$^+$	0.498	0.486	0.268	0.266	0.475	0.459
CONTRIQUE	0.629	0.648	0.451	0.544	0.591	0.598
Re-IQA	0.648	0.656	0.176	0.257	0.540	0.524
GRepQ	0.721	0.742	0.440	0.542	0.631	0.610
IPCE	0.816	0.831	0.459	0.548	0.731	0.713
GenzIQA	0.793	0.806	0.653	0.757	0.661	0.641

20K database. For cross-database evaluation, we choose rest of the AIGI databases viz. AGIQA-3K (Li et al., 2023b), AGIQA-1K (Zhang et al., 2023b) and AIGCIQA2023 (Wang et al., 2023b). We benchmark GenzIQA against other state-of-the-art quality representation learning methods such as CONTRIQUE (Madhusudana et al., 2022b), Re-IQA (Saha et al., 2023), GRepQ (Srinath et al., 2024), IPCE (Peng et al., 2024) and report the analysis in Tab. 17. We observe that our method performs consistently well across multiple generative IQA databases.

A.6 Different Variants of Stable Diffusion

As argued in the implementation details, we choose the input images and video frames resolution to the VQ-VAE as 512×512. Here, we analyze the impact of our choice in resolution on quality estimation. In Tab. 18, we study the impact on downscaling by comparing the performance at 512×512 with 256×256. We train GenzIQA on two different datasets viz. KonIQ-10K (official test-split) and CLIVE and test in a cross-database setting. While training and inference become $4\times$ faster at 256×256, the performance drastically deteriorates over all the train-test settings. We conclude that the higher resolution model is a better choice for significant performance gains even though the inference time is slower. Again choosing a variant with higher resolution than 512×512 will require more compute than a 24 GB commercial GPU.

A.7 Details of Datasets

A.7.1 Image Quality Assessment Datasets

To validate the generalizable capability of GenzIQA and other NR-IQA methods, we consider various datasets for training and evaluation purpose. These datasets are chosen to cover camera-captured, GAN restorted images, night-time captured and synthetically distorted image databases. In Tab. 19 we have given a comprehensive description of these databases.

A.7.2 Video Quality Assessment Datasets

To train and evaluate GenzVQA and other NR-VQA methods, we perform various experiments on publicly available VQA databases. These databases cover diverse categories of videos, such as user-generated content (UGC), including camera-captured videos, streaming content, high frame rate, ultra-HD, and gaming. Table 20 gives a comprehensive analysis of these databases.

Table 18: SRCC performance comparison of GenzIQA for different Stable Diffusion variants. Stable Diffusion v2 with two VQ-VAE variants feeding 256×256 and 512×512 sized images are considered.

Resolutions	**Train on CLIVE**				
	KonIQ$_{test}$	**NNID**	**CSIQ**	**LIVE-IQA**	**FLIVE$_{test}$**
256×256	0.653	0.725	0.567	0.629	0.362
512×512	0.750	0.738	0.664	0.782	0.454
Resolutions	**Train on KonIQ**				
	CLIVE	**NNID**	**CSIQ**	**LIVE-IQA**	**FLIVE$_{test}$**
256×256	0.700	0.776	0.533	0.592	0.445
512×512	0.793	0.782	0.658	0.788	0.489

Table 19: Summary of publicly available IQA datasets for GenzIQA analysis.

Dataset	# Images	Resolution	Image Category
FLIVE (Ying et al., 2020a)	39810	160p-700p	Camera-captured
KonIQ-10K (Hosu et al., 2020)	10073	768p	Camera-captured
CLIVE (Ghadiyaram & Bovik, 2015)	1162	500p-640p	Camera-captured
SPAQ (Fang et al., 2020)	11125	1080p-4368p	Camera-captured
PIPAL (Gu et al., 2020)	23200	288p	GAN-restored
NNID (Hu et al., 2021)	1340	512p	Night-time captured
CSIQ (Larson & Chandler, 2010)	866	512p	Synthetically distorted
LIVE-IQA (Sheikh et al., 2006)	779	480p-512p	Synthetically distorted
TID (Ponomarenko et al., 2015)	3000	384p	Synthetically distorted

Table 20: Summary of publicly available VQA datasets for GenzVQA analysis.

Dataset	# Videos	Duration (secs)	Spatial Resolution	Frame Rate	Video Category
LSVQ (Ying et al., 2021)	38,811	5-12	$\leq$ 4K	60	UGC
KoNVid-1K (Hosu et al., 2017)	1200	8	540p	24,25,30	UGC
LIVE-VQC (Sinno & Bovik, 2019)	585	10	1080p	30	UGC
Youtube-UGC (Wang et al., 2019)	1200	20	360p-4K	30	UGC
MaxVQA (Wu et al., 2023c)	4543	4-5	240p-1080p	$\leq$ 60	UGC
Live-Qualcomm (Ghadiyaram et al., 2018)	208	15	1080p	30	UGC
Waterloo-IVC -4K (Li et al., 2019b)	1200	9-10	540p, 1080p, 4K	24,25,30	Ultra-HD
LIVE YT-HFR (Madhusudana et al., 2021)	480	6-10	1080p	24,30,60, 82,90,120	Frame-rate Variation
LIVE YT-Gaming (Yu et al., 2022)	600	8-9	360p-1080p	30,60	Gaming
CGVDS (Zadtootaghaj et al., 2020)	367	30	480p,720p, 1080p	20,30,60	Gaming
CSIQ-VQD (Vu & Chandler, 2014)	180	10	480p	$\leq$ 60	Streaming
MD-VQA (Zhang et al., 2023c)	3762	8	720p, 1080p	$\leq$ 60	Streaming